Inferring fault mechanical conditions from the source parameters of a complex microseismic multiplet in the Corinth rift, Greece

Pierre Dublanchet, Maxime Godano, Pascal Bernard

AGU PUBLICATIONS

JGR

Journal of Geophysical Research: Solid Earth

RESEARCH ARTICLE
10.1002/2015JB012259

This article is a companion to *Godano et al.* [2015], doi:10.1002/2015JB012217.

Key Points:
- Mechanical modeling of a persistent multiplet
- Coseismic slip on complex multiplets could be used as creep meters
- The use of complex multiplets as creep meters requires a sufficient number of observations

Correspondence to:
P. Dublanchet,
pierre.dublanchet@gmail.com

Citation:
Dublanchet, P., M. Godano, and P. Bernard (2015), Inferring fault mechanical conditions from the source parameters of a complex microseismic multiplet in the Corinth rift, Greece, *J. Geophys. Res. Solid Earth*, *120*, 7655–7682, doi:10.1002/2015JB012259.

Received 4 JUN 2015
Accepted 6 OCT 2015
Accepted article online 10 OCT 2015
Published online 14 NOV 2015

Inferring fault mechanical conditions from the source parameters of a complex microseismic multiplet in the Corinth rift, Greece

P. Dublanchet[1,2], M. Godano[2], and P. Bernard[2]

[1]Swiss Seismological Service, ETH Zürich, Zürich, Switzerland, [2]Institut de Physique du Globe de Paris, CNRS, Paris, France

Abstract We develop a mechanical model of tight clusters of coplanar seismic asperities, to investigate a particular microearthquake swarm located at 8 km depth in the Corinth rift in Greece, which was active between 2001 and 2007. Although it is classified as a multiplet based on waveform similarity, this seismic sequence is much more complex than a repeating earthquake sequence and cannot be interpreted as the regular failure of a single asperity forced by surrounding aseismic creep. Here we suggest that such complex sequences could be generated by the failure of a set of coplanar asperities interacting in a small region of a fault segment. We show that in order to reproduce the dynamics of the observed sequence and the characteristics of the events, the cluster of asperities has to be located very close to an aseismically slipping fault segment, which could be an updip extension of the deep detachment zone in the rift, creeping at 1.5 cm/yr. For more general cases of coplanar clustered asperities, we show that the shape of the cumulative coseismic displacement pattern associated with the repeated failures of the asperities is strongly controlled by the behavior of the fault area surrounding the asperity cluster. In particular, if the cluster is part of a locked fault area, the resulting long-term cumulative displacement is maximum at the center of the cluster. In contrast, an asperity cluster surrounded by aseismic creep leads to a uniform cumulative coseismic slip pattern. The ratio between cumulative slip at the center of the seismogenic patch and cumulative slip at its periphery could therefore be an indicator of the mechanical conditions prevailing on the fault. A systematic study of the source parameters of complex microseismic sequences could therefore provide insights into the mechanical state of active faults continuously generating microseismicity.

1. Introduction

Since the discovery of repeating earthquakes in various places around the world [*Nadeau et al.*, 1995; *Bürgmann et al.*, 2000; *Matsuzawa et al.*, 2002; *Peng and Ben-Zion*, 2005], many microseismicity studies have focused on these particular sequences, which can be thought of as the periodic rupturing of a unique fault asperity. In spite of their scarcity in the global microseismicity records [*Igarashi et al.*, 2003; *Chen et al.*, 2007, 2003, 2010], the detailed analysis of these particular events has significantly contributed to the understanding of fault behavior, as soon as it has been suggested that the failure of these asperities could be forced by nearby aseismic slip [*Nadeau et al.*, 1995; *Nadeau and McEvilly*, 1999; *Beeler et al.*, 2001]. In particular, the estimation of the recurrence rate of repeating events on the San Andreas Fault allowed *Schaff et al.* [1998] to demonstrate the importance of aseismic slip in the postseismic deformation of the Loma Prieta earthquake. Furthermore, by similar analysis, *Nadeau and McEvilly* [1999], *Igarashi et al.* [2003], and *Lengliné and Marsan* [2009] were able to map interseismic aseismic deformation, as well as coseismic static stress redistribution on major plate boundaries.

A closer look at the groups of events generating similar waveforms (hereafter called multiplets) indicates that seismic failure on an asperity could be aperiodic, depending on the degree of interaction between neighboring sources [*Lengliné and Marsan*, 2009; *Chen et al.*, 2010, 2013]. Moreover, these clusters of small earthquakes sometimes involve more than one asperity. Such complex clusters have, for instance, been reported in the Parkfield area [*Lengliné and Marsan*, 2009; *Dublanchet et al.*, 2013a] and constitute the main feature of the seismic activity recorded in the Gulf of Corinth [*Lambotte et al.*, 2014; *Godano et al.*, 2014, 2015].

The present study focuses on these particular complex multiplets and aims at understanding the mechanical properties of faults that could be inferred from their analysis. To do so, we considered multiplet 866, a specific sequence observed between 2001 and 2007 in the continental rift of Corinth (Greece),

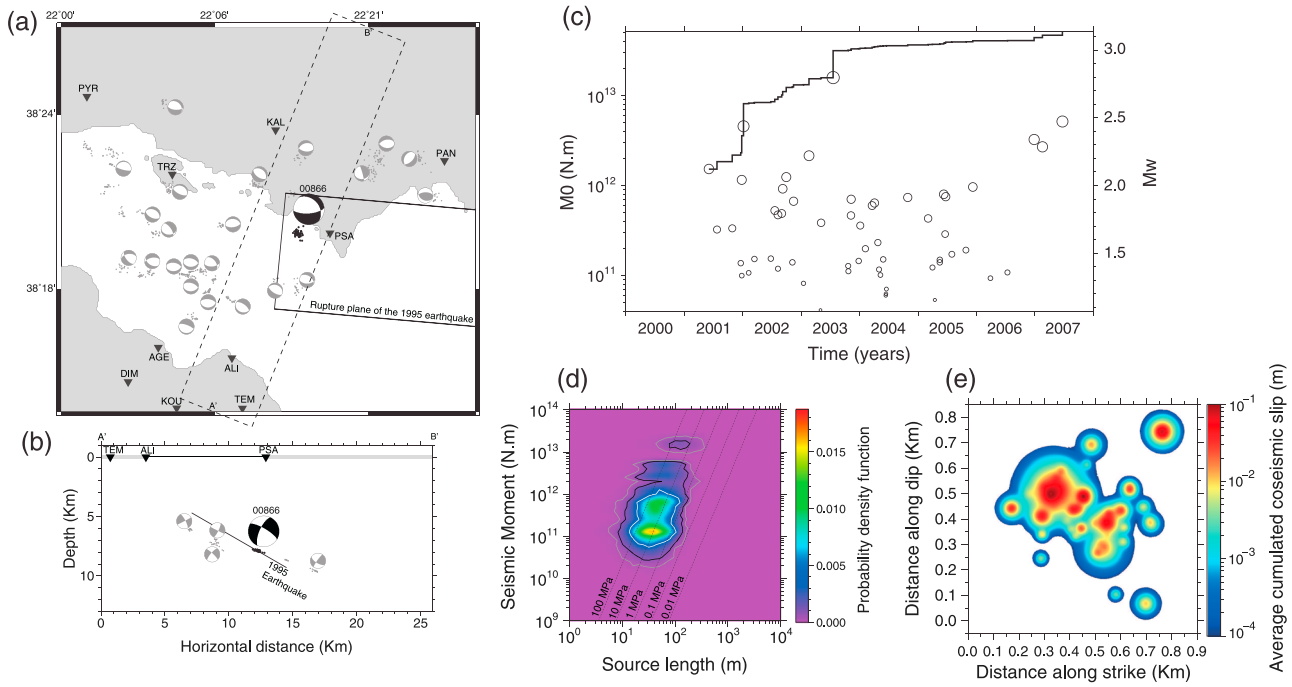

Figure 1. (a) Map view of the principal multiplets (dots) active in the western part of the Corinth rift between 2001 and 2007 [*Lambotte et al.*, 2014] and their composite focal mechanisms determined by *Godano et al.* [2014]. Permanent network stations are indicated with black triangles. The multiplet 866 analyzed here is outlined in black. (b) Cross section along the profile A′B′ shown in Figures 1a. (c) Sequence of events from the multiplet 866. Dots indicate the magnitude M_w of the events, and solid line indicates the cumulative coseismic moment M_0. (d) Scaling law characterizing the sequence presented in Figure 1c, derived from the analysis of *P* and *S* waves power spectra by *Godano et al.* [2015]. The probability density function (pdf) has been computed by resampling of the possible source parameters, accounting for all the uncertainties. Dashed black lines correspond to the theoretical scaling $M_{0s} = 2/7\Delta\tau L_s^3$ between the seismic moment M_{0s} and the rupture length L_s for different values of the stress drop $\Delta\tau$ indicated along the black lines. (e) Average cumulative coseismic displacement associated with the sequence in Figure 1c, obtained by resampling of the possible source parameters accounting for all the uncertainties. All these figures are from *Godano et al.* [2015].

where seismicity is associated with a N-S extension of 1.5 cm/yr accommodated along a low-angle detachment zone at 6–8 km depth [*Lambotte et al.*, 2014; *Godano et al.*, 2014]. We performed numerical simulations with the asperity model developed by *Dublanchet et al.* [2013a] in order to model first-order features of this particular sequence. The 7 year period between 2001 and 2007 corresponds to the first years of seismicity monitoring within the Corinth area by the Corinth Rift Laboratory (CRL) network [*Bernard et al.*, 2006]. Before and after this period, data are either not available or not yet analyzed. Figure 1 indicates the main characteristics of multiplet 866 proposed by *Godano et al.* [2015]. The characteristics can be summarized as follows: (1) a succession of 56 events with magnitudes ranging between 1.1 and 2.9 ruptured patches (asperities) within a 1 km long planar structure dipping approximately at 30° to the north and situated on the western edge of the inferred rupture plane of the 1995 M_w6.2 Aigion earthquake [*Bernard et al.*, 1997; *Godano et al.*, 2014], (2) a scatter of 2 orders of magnitude in the possible stress drops (between 1 and 100 MPa) of the events, and (3) a cumulative coseismic slip of the order of 10 cm. The Bayesian inversion of the spectral ratios conducted by *Godano et al.* [2015] allowed to estimate probability density functions for all the source parameters of these events. The results presented in Figures 1d and 1e were obtained by resampling all these probability density functions and therefore rigorously account for all the uncertainties associated with the source parameter estimation. The slip distribution shown in Figure 1e also accounts for the relative location error of 10–20 m in this part of the Corinth rift [*Lambotte et al.*, 2014; *Godano et al.*, 2015].

More precisely, the purpose of this study is first to use the source parameters provided by *Godano et al.* [2015] to infer whether the detachment zone of the Corinth rift is locally creeping or locked and in a broader sense to demonstrate how complex multiplets may help assess the occurrence of aseismic creep within active fault zones. To do so, we use the mechanical model of *Dublanchet et al.* [2013a] to infer the frictional conditions of the source region that under constant tectonic loading could generate sequences similar to that observed in Corinth. In particular, we study three different families of models. The first one is a cluster of asperities embedded in a creeping fault, the second is the same cluster embedded in a locked fault zone, and the last

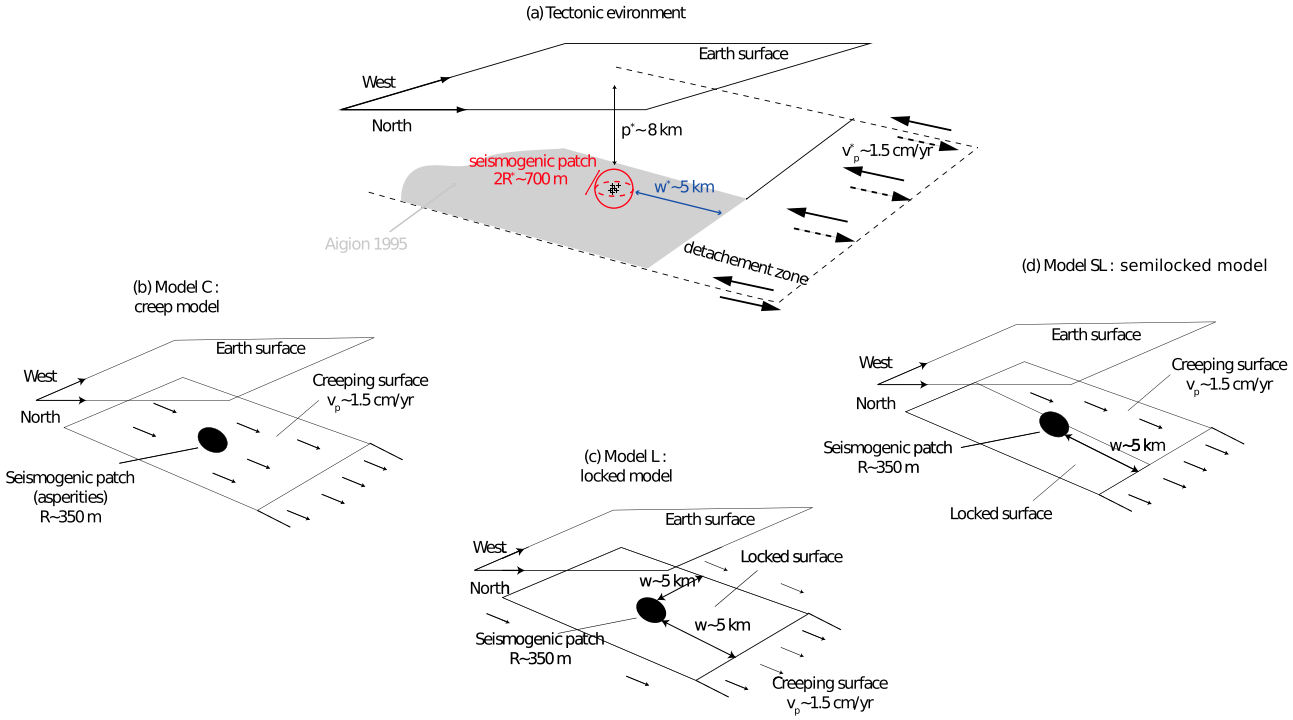

Figure 2. (a) Schematic diagram of the principal structures of the Corinth Rift in the region of the multiplet 866. The multiplet (black crosses) lies on a north dipping fault segment of characteristic dimension R^* at a depth p^* on the edge of the rupture area of the 1995 M_w6.2 Aigion earthquake represented by the gray area. The source region of the multiplet undergoes a stressing rate $\dot{\tau}^*_{tect}$ associated with the aseismic downdip shear detachment zone situated at a distance w^* from the multiplet, and accommodating a relative displacement at a constant rate v^*_p, as indicated by the black arrows. (b–d) Three end-member conceptual models of the multiplet environment: in model *C* the seismic sources (asperities) are surrounded by a creeping area extending the deep detachment zone; in model *L*, the asperities fail inside a locked fault segment; and in model *SL* the asperities lie in the transition zone between a locked and a creeping fault segment.

one is a cluster of asperities at the transition between a locked and a creeping fault segment. Instead of trying to model the exact succession of events in time, magnitude, and location, we draw comparisons between first-order features of observed and modeled sequences, such as the distribution of interevent time delays, the magnitude frequency distribution, the scaling between seismic moment and source size, the shape of the coseismic slip distribution, and the amplitude of the accumulated slip, as presented in Figure 1. The purpose here is to analyze the synthetic catalogs generated by the three categories of mechanical models in a statistical way, in order to estimate, for each model, the probability of being properly rejected by the data. This approach allows to evaluate in the case of Corinth or in a more general tectonic environment if the microseismicity is consistent with the presence of aseismic creep and if not to identify larger-scale asperities.

The remaining text is organized as follows: after a brief description of the seismotectonic context of the multiplet 866, the different families of end-member conceptual mechanical models are introduced. Then, we recall the main features of the numerical model of *Dublanchet et al.* [2013a] used in this study as an equivalent model for the multiplet source region. The synthetic catalog analysis procedure is introduced in section 3. Section 4 is dedicated to the comparison between synthetic sequences and the multiplet 866. In section 5, we further analyze the coseismic slip distributions produced by the different model categories, and a criterion based on the shape of the cumulative coseismic slip is derived to separate creeping and locked fault conditions.

2. Multiplet Modeling

2.1. Conceptual Model and Equivalent Mechanical Model

A schematic view of the tectonic environment of multiplet 866 is represented in Figure 2a. In the following, we assume that the events of the multiplet occurred in an elastic space, on a small patch of half-dimension $R^* \sim 350$ m situated on a planar fault segment dipping at 30° toward the north, as inferred from the distribution of hypocenters and the composite focal mechanism shown in Figures 1a and 1b [*Lambotte et al.*, 2014; *Godano et al.*, 2014]. As shown in Figures 1d and 1e, the minimum dimension of the asperities h^* is of the

Table 1. Characteristic Quantities of the Natural System Studied (Corinth Rift) and Parameters of the Equivalent Mechanical Model Deduced From These Characteristic Quantities

Characteristic Quantities	Value
Distance to the detachment zone w^*	~2.5–5 km
Seismogenic patch size R^*	~350 m
Smallest rupture length h^*	~10–20 m
Possible detachment creep rate v_p^*	15 mm yr^{-1}
Effective normal stress σ^*	~235 MPa
Parameters of the Model	
Elastic slab thickness w	10 km
Fault dimension L	1.92 km
Source region radius R	320 m
Elementary asperity size h	15 m
Number of asperities in the seismogenic patch n_{asp}	1433
Loading rate v_p	4.75×10^{-10} m s^{-1} ~15 mm yr^{-1}
Effective normal stress σ	235 MPa
Lame parameters $\lambda = \mu$	30 GPa
Radiation damping η	5×10^6 Pa s m^{-1}
Reference friction coefficient μ_0	0.6

order of 10 to 20 m. The depth p^* of this source region is 8 km, and it is situated near the western edge of the 1995 M_w6.2 Aigion earthquake as proposed by *Bernard et al.* [1997]. We further assume that the source region of this multiplet is loaded by the opening of the rift, that could be interpreted from the surface GPS measurements as either resulting from silent slip at constant rate $v_p^* \sim 15$ mm/yr on a detachment zone located downdip to the inferred rupture area of the Aigion earthquake, or as a consequence of a mode I steadily opening structure below the region of seismic activity [*Briole et al.*, 2000; *Bernard et al.*, 2006; *Lambotte et al.*, 2014]. In each model, the multiplet source region is situated at a distance w^* from the source of tectonic loading, which could be estimated roughly between 2.5 km (distance to the downdip edge of the 1995 rupture) and 5 km (distance to the downdip edge of the seismicity [*Lambotte et al.*, 2014]). All the characteristic dimensions of this zone are summarized in Table 1.

As $R^*/w^* \sim 0.1 \pm 0.05$ and $R^*/p^* \sim 0.05$, we assume that the source volume undergoes an almost uniform effective normal stress and a uniform stressing rate $\dot{\tau}^*_{\text{tect}}$ generated by the detachment zone. In order to get an order of magnitude for $\dot{\tau}^*_{\text{tect}}$, we assume that the deep detachment acts in an elastic medium as a shear dislocation, steadily creeping at a rate v_p^*. Assuming that the seismogenic patch and the dislocation are approximately coplanar, at a distance w^* from each other, $\dot{\tau}^*_{\text{tect}}$ is approximately given by

$$\dot{\tau}^*_{\text{tect}} \sim \frac{\mu'}{2\pi w^*} v_p^*, \tag{1}$$

where μ' is a function of the shear modulus μ and the Poisson ratio ν of the surrounding rock volume. $\mu' = \mu$ for antiplane strain and $\mu' = \mu/(1-\nu)$ for in-plane strain.

From the geodetic surface measurements [*Briole et al.*, 2000], and the relocation of microseismic activity [*Lambotte et al.*, 2014], it is impossible to determine precisely the mechanical conditions prevailing on the fault segment activated by the multiplet, and therefore, we consider successively three end-member models depicted in Figures 2b–2d: a creeping fault (model *C*), a locked fault (model *L*), and a semilocked model (model *SL*). In the semilocked model, the multiplet is located at the transition between a locked fault and a creeping fault. As shown later, we chose the mechanical parameters in models *C* and *SL* so that the creep rate on the aseismic segments is of the order of the deep detachment creep rate (1.5 cm/yr).

In order to study the behavior of such a source region, we consider the equivalent system shown in Figure 3a of a planar fault of dimension L embedded in a homogeneous elastic slab of thickness w. Slip u on the fault is constrained in the x direction, and it is resisted by rate-and-state friction [*Dieterich*, 1979; *Ruina*, 1983], so that frictional strength deviates from a constant friction coefficient μ_0 with the evolution of slip rate and slip

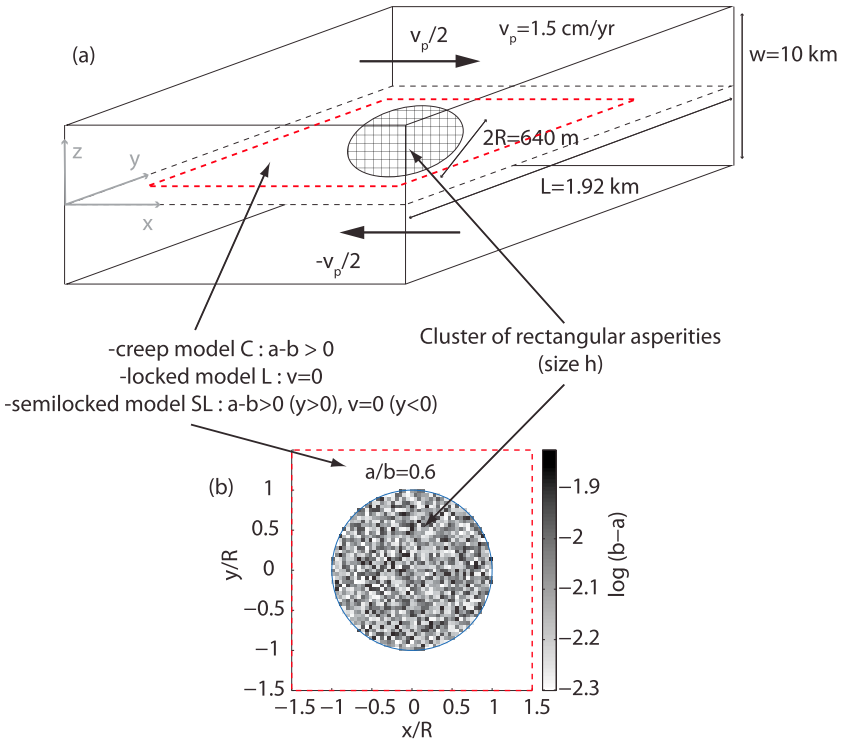

Figure 3. (a) Equivalent model for the source region of the multiplet 866. A circular set of square asperities (seismogenic patch) is centered on a planar fault segment of dimension L. The asperities are characterized by velocity-weakening frictional properties ($a - b < 0$). The boundary conditions on the surrounding area of the fault segment are either velocity strengthening properties ($a - b > 0$) allowing creep (creep model C), constrained against any slip (locked fault model L), or mixed between these two conditions (semilocked model SL). This system is loaded by an imposed motion at a constant rate v_p, at a distance $w/2$ in the fault normal direction. (b) Frictional structure ($b - a$ frictional parameter) of the seismogenic patch. Each square cell of dimension h corresponds to an individual computational cell and to an asperity as well. The total number of asperities within the seismogenic patch is $n_{asp} = 1433$. The frictional structure is here heterogeneous and corresponds to the seismogenic patch *IX* described in Table 2.

history along the interface which could be parametrized by two nondimensional coefficients a and b and a characteristic slip distance d_c. Furthermore, the slip history dependence is described by the slip version of the state evolution law [*Ruina*, 1983]. As discussed previously, we assume for simplicity that this fault segment undergoes a uniform normal stress σ and stressing rate $\dot{\tau}_{\text{tect}}$. In order to reproduce the stressing rate associated with the opening of the rift, the fault parallel boundaries of the elastic slab are forced to move at a constant rate $\pm v_p/2$ in the $\pm x$ direction, so that the plane $z = 0$ experiences a stressing rate $\dot{\tau}_{\text{tect}}$ given by

$$\dot{\tau}_{\text{tect}}(t) = \frac{\mu}{w}\left[v_p - v_m(t)\right], \tag{2}$$

where again, μ is the shear modulus of the elastic space, t is time, and $v_m(t)$ is the spatial average of the sliding velocity on the fault plane defined as $v(x, y, t) = \dot{\delta}(x, y, t)$ where $\delta(x, y, t) = u(x, y, 0^+, t) - u(x, y, 0^-, t)$.

The parameters of the equivalent mechanical model are listed in Table 1. The geometrical parameters R and h are chosen as orders of magnitude of the dimensions R^* and h^* characterizing the multiplet 866 (Table 1) [*Briole et al.*, 2000; *Lambotte et al.*, 2014; *Godano et al.*, 2015]. The rate v_p is equal to v_p^* in order to maintain an average creep rate on the creeping segments of the order of 1.5 cm/yr. Furthermore, we use $w = 10$ km, so that the stressing rate $\dot{\tau}_{\text{tect}}$ in our model (equation (2)) is of the same order of magnitude as the stressing rate imposed by the deep detachment zone $\dot{\tau}^*_{\text{tect}}$ (equation (1)), assuming $v_m = 0$. Since the evolution of the system is computed with the asperity model developed by *Dublanchet et al.* [2013a], we choose the spatial period of the system L so that $L < 2w$ which minimizes the error introduced by the use of a full space green function in the computation of the elastic interactions [*Dublanchet et al.*, 2013a]. We also ensure that $L > 4R$ which is a necessary condition to neglect the interactions with the periodic replicas of the source

[*Dublanchet et al.*, 2013a]. The normal stress σ used in our simulations is an order of magnitude of the expected lithostatic stress at 8 km depth, assuming a rock density of 3000 kg m^{-3}.

All the rate-and-state parameters μ_0, d_c, a, and b used here are chosen as far as possible in the typical range of the laboratory-derived rate-and-state parameters [*Marone*, 1998]. However, some of them, especially $b-a$ parameters, are somewhat larger than the laboratory values. This choice will be justified below and further discussed in section 6.

In order to model the seismogenic patch on the $z = 0$ plane, we assume a population of n_{asp} asperities distributed on a disk of radius R surrounded by a region either characterized by velocity strengthening friction properties (positive $a-b$ rate-and-state friction parameter), which enables stable creeping behavior (models *C* and *SL*) or constrained against any slip ($\dot{\delta} = 0$, for models *SL* and *L*). In the following, we describe successively the way the seismogenic patch and its fault environment are modeled.

2.2. Seismogenic Patch Structure

We adopt a discrete modeling approach in order to define the asperities [*Rice*, 1993]: each asperity is represented by a square velocity-weakening ($a-b<0$) computational cell oversized with respect to the critical length allowing unstable slip to occur on a rate-and-state interface, so that each asperity can dynamically fail as an earthquake independently from each other. In other words, we assume a unique size of elementary asperity (or computational cell) denoted h which verifies on each point of the fault $h > h_c$ where h_c is given in terms of the rate-and-state parameters by *Rice* [1993] as

$$h_c = \frac{\mu d_c}{(b-a)\sigma}. \tag{3}$$

A discontinuous approach allows to decrease significantly the computational cost, but as a drawback, the nucleation of instabilities on each elementary asperity is poorly described. However, the purpose of this study is to analyze the collective average behavior of a group of asperities and not the nucleation of each failure in detail. The second drawback of using a discrete description concerns the elastic stress interactions which depend on the computational cell size [*Dieterich*, 1995; *Ziv and Rubin*, 2003; *Ziv*, 2003]. This is related to the definition of the elastostatic kernel k_{ij} as the stress at the center of the cell j generated by a unit square dislocation occupying the cell i. Because of the decrease of stress with distance from the edges of the dislocation, the failure of a single computational cell generates a higher stress increase on its direct neighbors if the cell size is smaller. For large computational cells, the stress singularity ahead of a rupture front could therefore be underestimated, especially for small ruptures. In order to attenuate this cell size dependence of stress interactions, we follow *Ziv and Rubin* [2003] and compute k_{ij} as the average stress increase on the cell j generated by a unit dislocation on cell i, instead of the increase of stress at the center of the cell j.

In the following, we consider 10 different structures of seismogenic patch (labeled with the roman fonts I to X) for each model family *C*, *L*, and *SL*, which leads to 30 different mechanical models for the multiplet 866. All these structures are summarized in Table 2. In structures I to IV, all the asperities are characterized by the same a and b values. On the other hand, in structures V to X, a and b parameters are different for each asperity. In these heterogeneous structures, a and b are distributed within $[a_{min}; a_{max}]$ and $[b_{min}; b_{max}]$. All these distributions of a and b parameters are generated in the following way: we first determine a range of $b-a$ parameter that could lead to the range of stress drops observed by *Godano et al.* [2015], given the level of normal stress assumed in the model. This first estimation is based on the linear scaling between the stress drop and the $b-a$ parameter for a single degree of freedom elastic system [*Rice and Tse*, 1986]. Then we generate n_{asp} values of $b-a$ uniformly distributed within this range (one value for each asperity), and assuming a constant ratio a/b, we compute for each asperity an a and b parameter. As a consequence, all the seismogenic patches are characterized by different values of a/b. Finally, patches VI and VII are obtained by operating a permutation of the locations of the asperities within the seismogenic patch V, in order to evaluate how important the spatial distribution of the heterogeneity is in the interaction processes.

2.3. External Fault Region

Around the seismogenic patch, the fault is either locked (models of type *L* and *SL*) or aseismically creeping (models of type *C* and *SL*). In order to allow aseismic slip to occur on the creeping segments, we assume velocity strengthening properties $a-b>0$. The acceleration and deceleration of the slip transients that might occur on the creeping regions influence the failure of the asperities. Using a discontinuous approach to model

Table 2. Frictional Parameters a, b, and d_c for the 10 Different Distributions of Asperities Used to Model the Seismogenic Patch and Important Nondimensional Quantities[a]

Patch Model	I	II	III	IV	V	VI	VII	VIII	IX	X
Heterogeneity	no	no	no	no	u.d.	u.d.	u.d.	u.d.	u.d.	u.d.
a_i/b_i	0.2	0.4	0.6	0.8	0.2	0.2	0.2	0.4	0.6	0.8
$a_{i,\min}$	0.0025	0.007	0.015	0.04	0.0013	0.0013	0.0013	0.0033	0.0075	0.02
$a_{i,\max}$	0.0025	0.007	0.015	0.04	0.0037	0.0037	0.0037	0.01	0.0225	0.06
$b_{i,\min}$	0.0125	0.017	0.025	0.05	0.0062	0.0062	0.0062	0.0083	0.0125	0.025
$b_{i,\max}$	0.0125	0.017	0.025	0.05	0.0187	0.0187	0.0187	0.025	0.0375	0.075
$(b_i - a_i)_{\min}$	0.01	0.01	0.01	0.01	0.005	0.005	0.005	0.005	0.005	0.005
$(b_i - a_i)_{\max}$	0.01	0.01	0.01	0.01	0.015	0.015	0.015	0.015	0.015	0.015
a_e	0.0135	0.018	0.026	0.051	0.02	0.02	0.02	0.0265	0.039	0.0765
b_e	0.0125	0.017	0.025	0.05	0.0185	0.0185	0.0185	0.025	0.0375	0.075
$a_e - b_e$	0.001	0.001	0.001	0.001	0.0015	0.0015	0.0015	0.0015	0.0015	0.0015
d_{ci} (mm)	0.2	0.2	0.2	0.2	0.2	0.2	0.2	0.2	0.2	0.2
d_{ce} (mm)	132	176.25	264.375	528.75	198	198	198	264	396	793.5
$h/h_{c,i,\max}$	5.88	5.88	5.88	5.88	2.93	2.93	2.93	2.93	2.93	2.93
$h/L_{b,e}$	0.01	0.01	0.01	0.01	0.01	0.01	0.01	0.01	0.01	0.01
$\frac{(1-\rho)(a_e-b_e)}{\rho(b_i-a_i)_{\max}}$	1.05	1.05	1.05	1.05	1.07	1.07	1.07	1.07	1.07	1.07

[a]The line entitled heterogeneity indicates if all the asperities of the seismogenic patch have identical frictional properties (no) or not. In the latter case, the distribution of $b-a$ on the seismogenic patch follows a uniform distribution (u.d.), with a and b in $[a_{\min}; a_{\max}] \times [b_{\min}; b_{\max}]$. Subscribe i refers to the seismogenic patch and subscribe e to the surrounding region. The size of one asperity (and the computational cell size) is h, h_c is the critical length given by equation (3), L_b is the characteristic length given by equation (4), and $\rho = \pi R^2/L^2$, where R is the seismogenic patch radius and L is the modeled fault length. The three bottom lines show that the conditions for a discrete description on the patch ($h/h_{ci} > 1$), a continuous description on its surroundings ($h/L_{be} < 0.05$), and global stability (positive spatial average of $a - b$) are satisfied for each asperity distribution.

such transients introduces a bias in the forcing of the asperities, since the amplitude, the spatial extent, and the duration of these aseismic slip events are not properly described [*Perfettini and Ampuero*, 2008]. Therefore, we use a continuous description for the regions of the fault surrounding the seismogenic patch, which means that each computational cell is much smaller than the minimum critical length L_b [*Dieterich*, 1992; *Perfettini and Ampuero*, 2008] given by

$$L_b = \frac{\mu d_c}{b\sigma}. \tag{4}$$

Since our simulations are performed with the slip version of the state evolution law, we ensure that the cell size h is even smaller than $0.05L_b$ [*Ampuero and Rubin*, 2008]. This mixed approach, with discontinuous conditions on the seismogenic patch ($h > h_c$) and continuous conditions on the surroundings of the patch ($h << L_b$) could be implemented assuming a unique computational cell size h, and using different d_c values for the seismogenic patch and the surrounding regions. Here we consider two different values of d_c, one for each region of the fault plane.

Rate-and-state parameters a and b are assumed constant on this region. The b parameter is arbitrarily set to the maximum b value on the seismogenic patch. Furthermore, our choice of a is guided by the previous work of *Dublanchet et al.* [2013a, 2013b], who demonstrated that faults characterized by a spatially variable $a - b$ (positive and negative) generate huge ruptures destabilizing the aseismic slip as soon as the spatial average of $a - b$ is negative. Since our goal is to compare the behavior of a seismogenic patch surrounded either by locked conditions or stable creep, we have to ensure that the average value of $a - b$ is positive. This condition is met if

$$(a_e - b_e) > \frac{\rho}{1-\rho}(b_i - a_i)_{\max}, \tag{5}$$

where $a_e - b_e$ is the $a - b$ value around the seismogenic patch, $(b_i - a_i)_{\max}$ the maximum value of $b - a$ within the seismogenic patch, and $\rho = \pi R^2/L^2$ the ratio between the seismogenic patch area and the total

area of the fault segment. All the frictional parameters characterizing the external region of the fault plane are summarized in Table 2.

In order to model a locked fault segment (in models *L* and *SL*), we artificially impose an almost vanishing slip rate on the external region of the fault. Furthermore, we increase the normal stress on this external region by a factor of 100 in order to prevent any slip acceleration during the period of time modeled.

Finally, the intermediate semilocked models *SL* are constructed assuming creeping conditions in the $y > 0$ domain of the fault, and locked conditions in the $y < 0$ domain, $(x = 0, y = 0)$ being the coordinates of the seismogenic patch center. The boundary separating the locked and the creeping segments within a semilocked model is thus parallel to the slip direction, as this is expected in the source region of the multiplet 866 (see Figure 2d).

3. Synthetic Catalog

The stress, slip, and seismic moment history of the interface are numerically computed using the quasi-dynamic asperity model developed by *Dublanchet et al.* [2013a] and a synthetic catalog of seismicity is constructed assuming that an event occurs each time the maximum slip rate on the fault v_{max} exceeds the seismic rate $v_{sis} = 1$ cm s^{-1}. This threshold could be compared to the slip rate v_{dyn} defined by *Rubin and Ampuero* [2005] as the minimum velocity allowing the dynamic effects to dominate over the direct effect of the friction law. v_{dyn} is given by

$$v_{dyn} = \frac{a\sigma}{\eta}, \tag{6}$$

where a is the direct effect rate-and-state friction parameter, and η is the damping parameter [*Rice*, 1993]. With the parameters reported in Table 2, v_{dyn} is larger than or equivalent to 6 cm s^{-1}, which is of the same order of magnitude than v_{sis}. The results presented below are not affected by this latter choice since the most significant effect of modifying v_{dyn} is to change the number of small magnitude events which will not be considered.

Each time an event is identified, all the asperities sliding at a rate larger than v_{sis} are considered to participate to the event. Then, for each asperity involved in a particular event, we compute a coseismic slip as the slip accumulated during the time lapse characterized by $v_{max} > v_{sis}$. The centroid of the earthquake is afterward computed as the barycenter of the coseismic slip distribution generated by the failure of all the participating asperities, and the size L_s is calculated as 2 times the maximum distance between the centroid and the four corners of each asperity involved in the rupture. The seismic moment released by one event M_{0s} is obtained as the difference between the total seismic moment released by the entire fault at the end of the rupture (when v_{max} first decreases below v_{sis}) and the total seismic moment at the onset of the rupture (when v_{max} first exceeds v_{sis}). A magnitude M_w is then computed from the definition of *Hanks and Kanamori* [1979]:

$$M_w = \frac{2}{3}\log M_{0s} - 6.0. \tag{7}$$

This approach allows to compute from a given mechanical model a synthetic seismic catalog containing for each event all the source parameters usually estimated for natural seismicity: timing, location, duration, size, coseismic moment released, magnitude, and slip distribution. For all the 30 models of multiplet, a synthetic catalog of several thousands of events is computed. However, in our analysis, we only consider the events occurring after an initial transient corresponding to the time needed for the average fault slip to reach a long-term steady state.

In the following sections, the synthetic catalogs generated by our 30 different models are first compared to the observed sequence of the multiplet 866 (section 4). Then the different catalogs are analyzed in a more general way (i.e., without accounting for the particularities of the multiplet 866), in order to develop a new method to distinguish between creeping and fully locked fault environments (section 5).

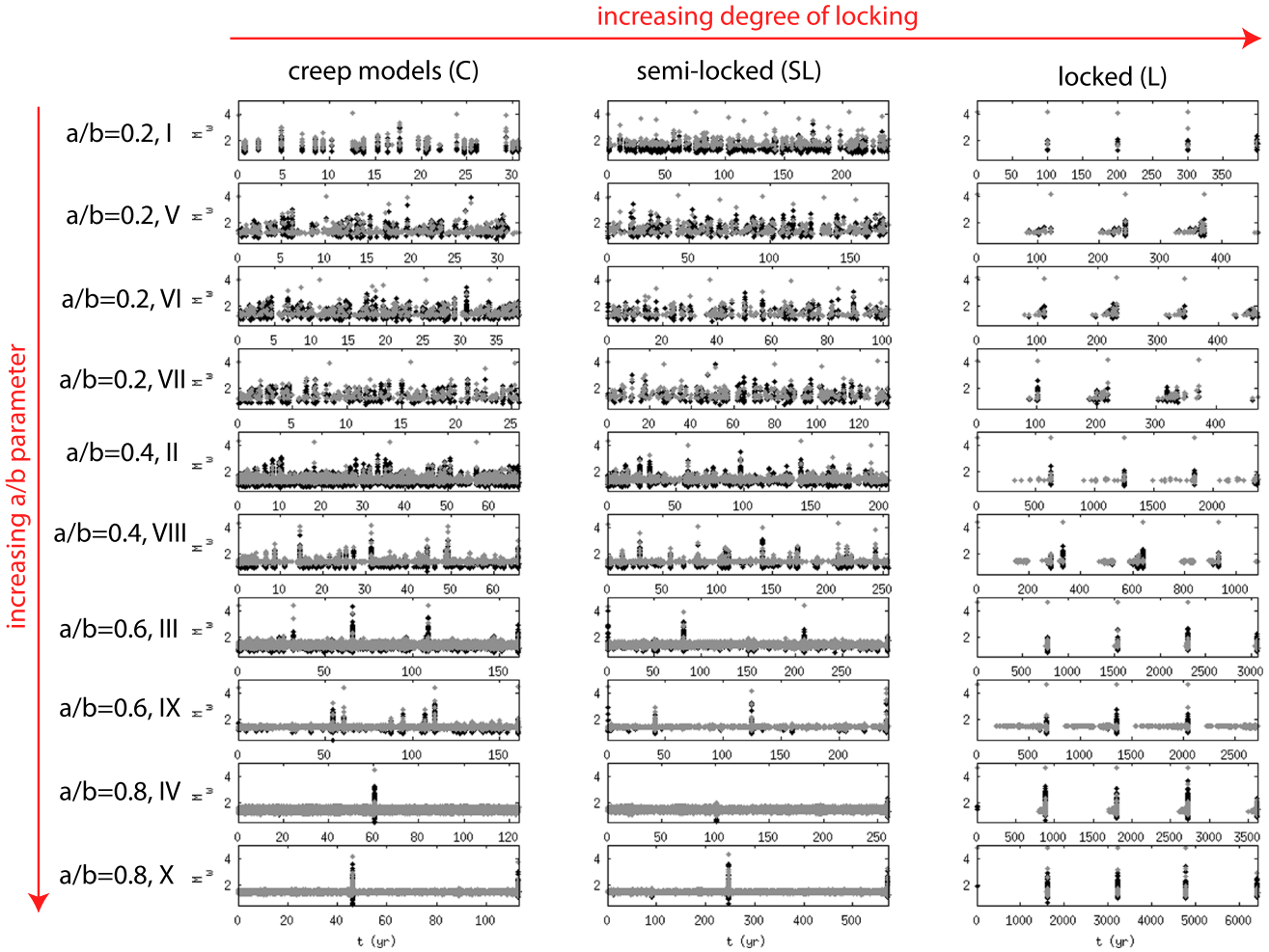

Figure 4. Raw seismic catalogs (black points), and catalogs after removing the undetectable events (gray dots) for each of the 30 models of the multiplet 866. Time is t, and M_w is the moment magnitude. All the subfigures of a same line correspond to the results obtained with the same seismogenic patch (I to X in Table 2), but with the different fault environments (*C*, *SL*, and *L*) presented in Figure 2. The subfigures are organized by increasing a/b parameter and increasing degree of locking on the fault environment.

4. Possible Mechanical Models for the Multiplet 866

4.1. Selection of Acceptable Sequences

In order to compare the synthetic catalogs to the observations, we first remove from the synthetic catalog all the events that might be hidden in the coda of previous events. For that, we assume a minimum time delay between events $\Delta t_{\min} = 100$ s, and for each event i of the catalog, we remove all the events j satisfying the following criterion:

$$\begin{cases} 0 < t_j - t_i < \Delta t_{\min} \\ M_{wj} < M_{wi} + 0.5, \end{cases} \tag{8}$$

where (t_k, M_{wk}) are the timing and the magnitude of event k. Our choice of $\Delta t_{\min} = 100$ s is motivated by the fact that 100 s is the minimum time delay between the events of the multiplet. The effect of $\Delta t_{\min}$ will be described in section 6. Furthermore, we assume that a magnitude difference of 0.5 is enough to separate two events within 100 s. However, this choice has no fundamental impact on the results presented below. For each one of the 30 models considered here, we represent in Figure 4 a piece of the raw synthetic catalog (without removing those undetectable events) along with the same sequence after the removal of the undetectable events. The figure is organized as a function of the a/b parameter on the seismogenic patch and the degree of mechanical locking on its surrounding region.

Table 3. Total Number n_S of **S** Sequences (Left Number) and Frequency n_Σ/n_S of $\boldsymbol{\Sigma}$ Sequences (Right Percentage) in the Catalogs Generated by the 30 Different Models (Seismogenic Patches I to X Described in Table 2, With Fault Conditions *C*, *L*, and *SL* Described in Figure 2)[a]

Model	a/b	Creep (*C*)	Semilocked (*SL*)	Locked (*L*)
I	0.2	4,823, 1.16%	5,405, 0.78%	1,736, 0.0%
V	0.2	6,022, **13.93**%	5,884, 0.54%	8,605, 0.0%
VI	0.2	5,235, **8.17**%	6,410, **3.10**%	7,753, 0.0%
VII	0.2	5,446, **20.0**%	5,638, 1.88%	7,783, 0.0%
II	0.4	12,210, **4.80**%	16,960, **5.23**%	22,124, 0.018%
VIII	0.4	7,848, **7.53**%	13,743, **3.37**%	1,517, 0.0%
III	0.6	26,833, 0.64%	21,592, 0.33%	29,368, 0.014%
IX	0.6	26,495, 0.004%	22,177, 0.0%	13,968, 0.26%
IV	0.8	45,301, 0.0%	42,174, 0.002%	6,676, 0.18%
X	0.8	49,659, 0.0%	28,334, 0.0%	16,427, 0.018%

[a]Frequencies higher than 3% are indicated with bold text.

In a second step, we remove all the events with a magnitude smaller than the smallest possible magnitude m observed in the multiplet 866 by *Godano et al.* [2015]. From the results presented in Figure 1c, and the uncertainty associated with the magnitude estimation, m is 0.93.

Within the remaining earthquakes, we identify all the n_S sequences of 56 successive events. That is, for a given initial event E_k, $k \in [1; n_S]$, we define the corresponding sequence S_k as

$$S_k = \left\{ E_i,\ i \in [k; k+55] \right\}. \tag{9}$$

Let us call **S** the set of all S_k, so that

$$\mathbf{S} = \left\{ S_k,\ k \in [1; n_S] \right\}. \tag{10}$$

However, only a fraction of the n_S sequences of **S** is characterized by magnitudes within the observed magnitude range. The subset $\boldsymbol{\Sigma}$ of **S** satisfying this magnitude content criterion is defined as follows:

$$\boldsymbol{\Sigma} = \left\{ S_k,\ k \in [1; n_S],\ \min_{E_i \in S_k} \left(M_{wi}\right) - m < \Delta m,\ 0 < M - \max_{E_i \in S_k} \left(M_{wi}\right) < \Delta m \right\}, \tag{11}$$

where m and M are, respectively, the minimum and maximum possible observed magnitude in the multiplet 866, and Δm the maximum error associated with the magnitude estimation. Here we have $m = 0.93$, $M = 2.86$, and $\Delta m = 0.4$ [*Godano et al.*, 2015]. Hereafter, we define the total number of sequences within $\boldsymbol{\Sigma}$ as n_Σ, and we will call **S** sequences and $\boldsymbol{\Sigma}$ sequences elements of **S** and $\boldsymbol{\Sigma}$, respectively. From these definitions, the sequence observed in the multiplet 866 is a $\boldsymbol{\Sigma}$ sequences.

For each model, the total number n_S of **S** sequences as well as the proportion n_Σ/n_S of $\boldsymbol{\Sigma}$ sequences within **S** are indicated in Table 3. The first result appearing from this table is that locked environments, as well as high values of a/b parameter within the seismogenic patch generate very few (or no) $\boldsymbol{\Sigma}$ sequences. These models could therefore be rejected at a high confidence level (more than 97%).

One possible explanation relies on the fact that high a/b patches do not generate as many large and intermediate magnitude events (with $M_w > 2$) as low a/b patches do (Figure 4). Parameters a and b indeed control the sensitivity of asperities to stress perturbations. A stress increase produces larger accelerations of slip on an asperity characterized by a small a value [*Dieterich*, 1979, 1992]. Parameter a being an increasing function of a/b for a given $b-a$ value, increasing a/b decreases the sensitivity of asperities to the failure of their neighbors. In turn, seismic ruptures have more difficulties to extend in the case of large a/b, which decreases the probability of generating large-magnitude events. This effect has already been observed in numerical discrete simulations by *Ziv and Cochard* [2006], who report a decrease of the slope of the magnitude-frequency distribution as the parameter a of the velocity-weakening region decreases and the corresponding parameter b increases (increasing the stress drop).

The reason for the absence of suitable $\boldsymbol{\Sigma}$ sequences generated with locked fault conditions is less obvious. In all the simulations conducted with such locked fault conditions, the seismicity occurs as periodic cycles consisting in a swarm of activity followed by a period of quiescence (Figure 4). During one swarm, the seismicity rate

and the maximum magnitude progressively increase, leading to a major event corresponding to the seismic rupture of the entire patch. We noticed (Figure 4) that the duration of the swarms and the rate of magnitude increase are both controlled by the a/b parameter. These features could be interpreted to the first order in terms of stress transfers between asperities: in this framework, a swarm corresponds to the progressive destabilization of the seismogenic patch as a cascade of events. This process could be compared to the nucleation of a slip instability on a homogeneous velocity-weakening fault [*Rubin and Ampuero*, 2005; *Ampuero and Rubin*, 2008], which can occur, depending on the a/b ratio in very different ways, from an expanding accelerating crack to a localized slip acceleration. Here again, the nucleation phase of large events on the seismogenic patch is controlled by the a/b parameter and the degree of heterogeneity between the different asperities. In these conditions, generating $\boldsymbol{\Sigma}$ sequences would require a very specific value of the a/b parameter, which we might not have tested in our simulations.

The story is extremely different when the seismogenic patch is located in the vicinity of a creeping fault segment. In addition to the stress transfers among the asperities, the interaction between asperities and the creeping sections of the fault has to be considered. This nonlinear process introduces a strong complexity in the seismicity patterns and seems to increase the probability of generating the observed magnitude range (Figure 4).

The second important feature outlined by the results reported in Table 3 is that the probability of generating $\boldsymbol{\Sigma}$ sequences is higher when considering heterogeneous $b-a$ distributions (structures V to VIII) than constant $b-a$ distributions (structures I and II). This occurs because the heterogeneity in $b-a$ introduces a heterogeneity in stress drops [*Rice and Tse*, 1986], so that all the asperities are not anymore able to trigger the failure of their neighbors. The heterogeneity therefore increases the amount of small events when strong interaction conditions prevail (low a/b) and thus increases the magnitude range observed. Furthermore, the presence of weak asperities failing in an isolated manner make small events more visible, because they are not always instantaneously triggered (or triggered less than 100 s after another event so that they would be eliminated by our catalog analysis). This could explain why patches with heterogeneous $b-a$ and $a/b=0.2$ (patches V to VII) produce much more $\boldsymbol{\Sigma}$ sequences than patches with a constant $b-a$ and the same ratio $a/b=0.2$ (patch I). This interpretation is further supported by the comparison between results obtained with patches V–VII: when reorganizing the spatial distribution of asperities, the environment of a particular asperity changes which in turn modifies the probability of generating $\boldsymbol{\Sigma}$ sequences.

In the following, we compare the different characteristics and source parameters of the $\boldsymbol{\Sigma}$ sequences obtained with the most productive models (i.e., with seismogenic patches generating more than 3% of $\boldsymbol{\Sigma}$ sequences in one of the fault conditions *C*, *SL*, or *L*), with the observations of the 56 events of the multiplet 866 reported in Figures 1c–1e. In particular, we will compare the scaling relationship between seismic moment M_{0s} and source size L_s, the magnitude-frequency distributions, the cumulative coseismic slip distribution, and the distribution of interevent time delays.

4.2. Comparing Synthetic and Observed Sequences

The comparison between observed and synthetic magnitude frequency distributions is conducted as follows. First, we compute this distribution for the observations, accounting for the error in the magnitude estimates. In other words, we generate samples of 56 magnitudes by randomly selecting for each event a magnitude within the range of possible magnitudes proposed by *Godano et al.* [2015]. Then we calculate for each magnitude bin the mean, maximum, and minimum number of events falling in this bin. We proceed in the same way to compute the average magnitude-frequency distribution generated by the models, by taking the mean distribution of all the $\boldsymbol{\Sigma}$ sequences generated and estimating for each magnitude bin the scatter in the proportion of events.

We perform similar resamplings to compute the interevent time delay distributions of the observed and modeled sequences. However, since the error in the timing of the events in the multiplet 866 is small (at most a few seconds), all the distributions generated for the data are similar.

Concerning the scaling relationship between seismic moment and source size, we compute the joint probability density function for M_{0s} and L_s obtained from analyzing all our modeled $\boldsymbol{\Sigma}$ sequences. This observed joint probability density is obtained by generating a population of samples consisting in 56 (M_{0s}, L_s) couples

(one for each event of the sequence), where the seismic moment is randomly selected within the range proposed by *Godano et al.* [2015] and the source size is selected according to the probability density function for source size determined by *Godano et al.* [2015].

Finally, each slip distribution is characterized by a shape parameter R_u defined as follows: If P is the barycenter of the cumulative coseismic slip distribution generated by 56 events, and $R_{\max}$ the maximum distance between P and any point on the fault that experienced slip during the sequence, R_u is given by

$$R_u = \frac{U_i}{U_e}, \tag{12}$$

where U_i is the cumulative coseismic slip averaged over the inner region of the patch (that is at a distance smaller than $0.5R_{\max}$ from P), and U_e the cumulative coseismic slip averaged over the external region of the patch (that is at a distance between $0.5R_{\max}$ and $R_{\max}$ from P). In order to generate distributions of R_u parameter for each model, we use the same sampling method as before. For one model, we compute one R_u value for each $\boldsymbol{\Sigma}$ sequence. Similarly, a R_u distribution for the data is computed. For that we generate a population of samples consisting in 56 four-component vectors (x, y, L_s, and U) (one for each event), where (x, y) is the location of the event, L_s its size, and U the associated amount of slip. Each component of the vector is selected within the range of possible values estimated by *Lambotte et al.* [2014] and *Godano et al.* [2015]. Then, a coseismic slip distribution, and the associated R_u, is computed from each sample of 56 four-component vectors.

4.3. A Creep Model for the Multiplet 866

4.3.1. Magnitudes and Source Size

The synthetic joint probability densities of the seismic moment M_{0s} and the source size L_s for the preferred models selected in the previous sections are represented in Figures 5 (column 1) and 5 (column 2), along with the theoretical relationship assuming constant stress drop $\Delta\tau$ [*Eshelby*, 1957]:

$$M_{0s} = \frac{2}{7}\Delta\tau L_s^3. \tag{13}$$

To the first order, all the synthetic sequences are approximately compatible with the constant stress drop model (equation (13)). Furthermore, the stress drops (i.e., the ratio between M_{0s} and L_s^3) for all the modeled sequences are between 1 and 100 MPa, which is the typical range observed in the multiplet 866 (Figure 1d). As shown in Figures $5a_1$, $5b_1$, and $5c_1$ and Figures $5a_2$, $5b_2$, and $5c_2$, in the range of frictional parameters assumed here, changing the organization of the asperities within a patch does not influence significantly the slope of the scaling trend nor the estimated stress drops. Similarly, assuming heterogeneous or identical asperities has no significant effect on the general shape of the scaling, as indicated by the comparison between Figures $5d_1$ and $5e_1$ and Figures $5d_2$ and $5e_2$.

The only difference arising from the heterogeneity or the use of different values of a/b on the fault patch is the way events distribute within the constant stress drop trend. This could be seen in the magnitude distributions shown in Figure 5 (column 3): if heterogeneous $b - a$ patches characterized by $a/b = 0.2$ are able to generate in each magnitude range as many events as observed (at least for magnitudes higher than 1.4 (Figures $5a_3$ to $5c_3$)), a higher a/b ratio concentrates the magnitudes between 1.2 and 1.6 (Figure $5d_3$). The magnitude range is further restricted by the use of identical asperities (Figure $5e_3$). Moreover, changing the a/b ratio seems to have more consequences on the magnitude distribution than reorganizing the asperity locations (Figure 5, column 3).

Note that heterogeneous models (structures V to VIII) overestimate the level of seismicity generated at magnitudes smaller than 1.4. This might indicate that the completeness magnitude in the multiplet 866 is of the order of 1.4, and therefore, some events are missing below this threshold. This issue will be further discussed later.

Finally, no significant difference appears in the distribution of magnitudes (or moments) and event size when changing from the creeping models to the semilocked models (Figure 5), meaning that both models could still be used to model the fault conditions prevailing in the source region of the multiplet 866. In other words, the scaling between M_{0s} and L_s is more strongly controlled by the interactions between the different sources than by the stressing rate, which is different in the two classes of models.

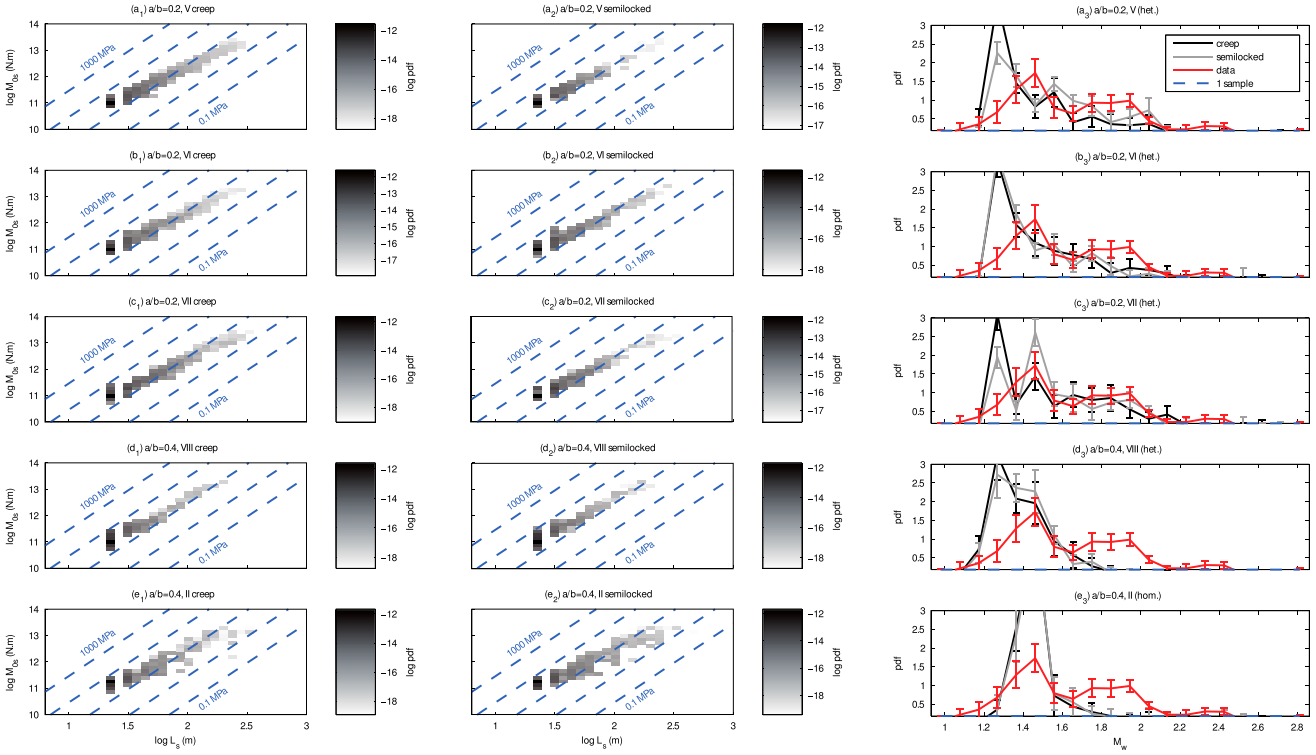

Figure 5. (columns 1 and 2) Modeled scaling relationship between seismic moment (M_{0s}) and source size (L_s) for $\boldsymbol{\Sigma}$ sequences. The models used here are indicated in the title of each subfigure. They all produce more than 3% of sequences similar to the observations (models highlighted in Table 3). Colors indicate the level of the probability density function computed for each model with all the $\boldsymbol{\Sigma}$ sequences. Blue lines indicate the constant stress drop model (equation (13)). Each blue line corresponds to a 10 times increase in the stress drop $\Delta\tau$ between 0.1 and 1000 MPa. (column 3) Corresponding magnitude-frequency distributions of observed (red) and modeled (levels of gray) $\boldsymbol{\Sigma}$ sequences. Black lines correspond to the marginal probability density function associated with the results in Figure 5 (column 1). Gray lines correspond to the marginal probability density function associated with the results in Figure 5 (column 2). The blue dashed line indicates the pdf associated with one sample per bin.

4.3.2. Coseismic Slip

The cumulative coseismic slip distributions generated by our preferred patch models, as well as the R_u distribution, are presented in Figure 6. Note that the diagrams in Figures 6 (column 1) and 6 (column 2) show examples of the slip distribution generated by one particular $\boldsymbol{\Sigma}$ sequence, whereas the R_u distributions shown in Figure 6 (column 3) provide a statistical information about the slip distribution generated by all observed and modeled $\boldsymbol{\Sigma}$ sequences.

For each model, the maximum cumulative coseismic slip is approximately 10 cm, which is similar to the observations (Figure 1e). Furthermore, in the sequences in Figure 6, the events (and thus the slip) concentrate in the periphery of the patch that is the closest to the creeping region (in the $y > 0$ domain for semilocked conditions). This region corresponds to the portion of the seismogenic patch experiencing the highest creep-related stressing rate. Therefore, for equivalent stress drops, asperities situated in this region fail more frequently. In contrast, the central part of the patch episodically compensates its slip deficit by larger but less frequent events, with magnitudes larger than 3. Such large-magnitude events are not observed in the multiplet 866, and by definition not present in the synthetic $\boldsymbol{\Sigma}$ sequences. From our simulation results, we suggest that these larger events compensating the slip occur between the different $\boldsymbol{\Sigma}$ sequences, which means that the observed sequence only partially activates the seismogenic patch.

In the case of fully creeping conditions (models *C*), the slip distributions present an annular shape (Figure 6, column 1), which becomes a semiannular shape in the presence of a locked segment (Figure 6, column 2). Between the two models, the barycenter of the coseismic slip distribution is translated in the $y > 0$ direction, which affects the R_u parameter distribution (Figure 6, column 3). This effect is more pronounced for small a/b values as shown in Figures $6a_3$ to $6c_3$, where the R_u distributions for semilocked conditions are concentrated

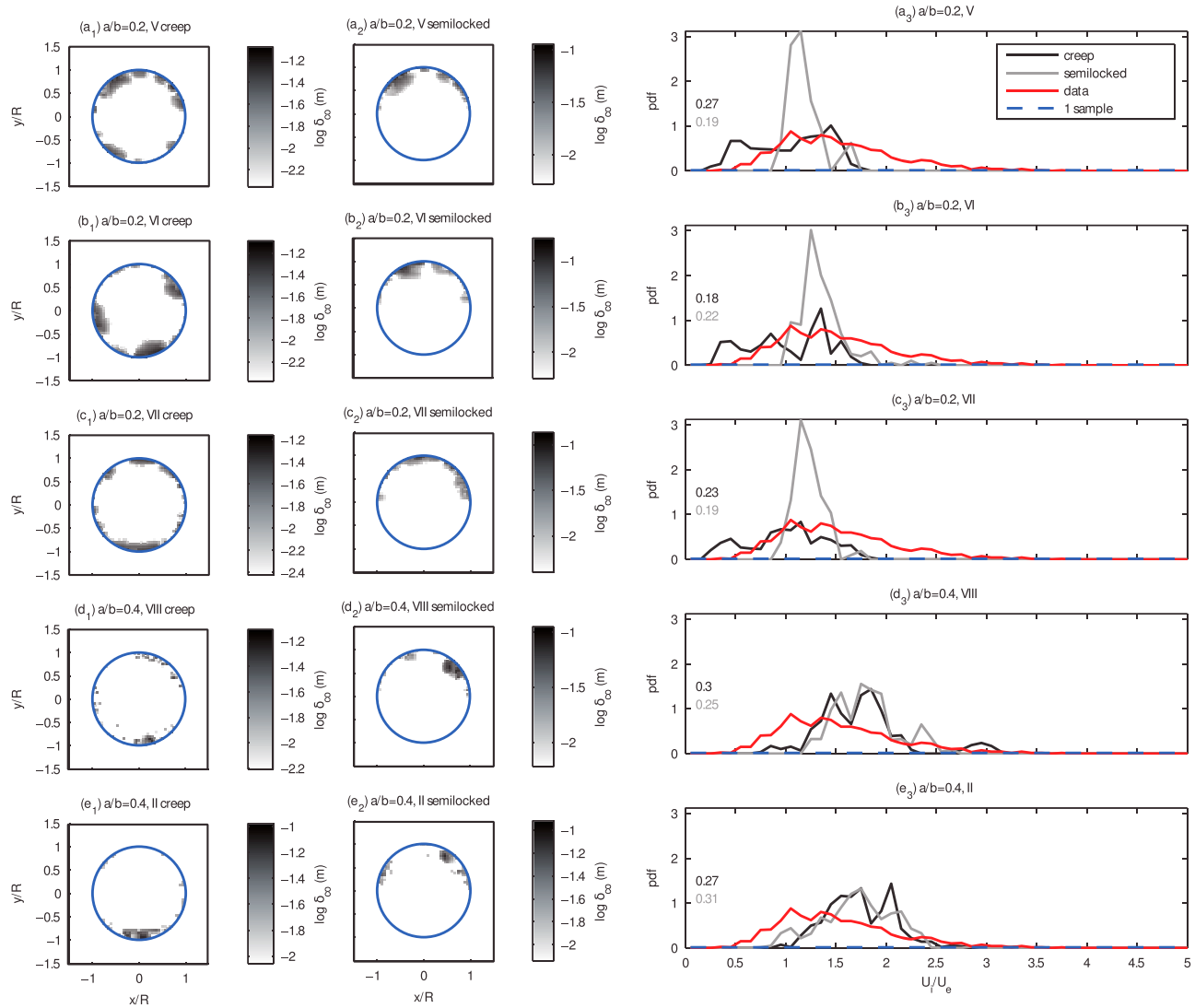

Figure 6. (columns 1 and 2) Modeled cumulative coseismic slip δ_{co} generated by one single $\boldsymbol{\Sigma}$ sequence on the seismogenic patch. The models used here are indicated in the title of each subfigure. They all produce more than 3% of sequences similar to the observations (models highlighted in Table 3). The blue circle indicates the extent of the seismogenic patch. The Cartesian coordinates on the fault plane are indicated by x and y as indicated in Figure 3. R is the radius of the seismogenic patch. For semilocked conditions (Figure 6, column 2), the creeping section is situated in the $y > 0$ domain, the $y < 0$ domain being fully locked. (column 3) Corresponding distributions of $R_u = U_i/U_e$ parameter of observed (red) and modeled (levels of gray) $\boldsymbol{\Sigma}$ sequences. The probability density function (pdf) for the data has been obtained according to the method described in section 4.2. Black and gray lines correspond to the pdf obtained from creeping and semilocked conditions, respectively. The blue dashed line indicates the pdf associated with one sample per bin. For each model, the probability of wrongly rejecting the model $\Pi_{d,m}$ (equation (A2)) is written in the top left corner of each figure. The same color scale is used for the distribution and the values of $\Pi_{d,m}$.

between $R_u = 1.0$ and $R_u = 1.5$, whereas the R_u distributions for creeping conditions spread over a broader range of R_u values, especially toward $R_u = 0$, which is expected when the slip distribution is perfectly annular ($U_i = 0$). This difference is less obvious for higher values of a/b (Figures 6d$_3$ and 6e$_3$).

Despite these differences, the comparison between the modeled and the observed R_u distributions does not allow to reject one model category or the other. In order to quantify this statement, we develop a simple statistical method presented in Appendix A, allowing to estimate the adequation between a model and data or, in other words, to estimate the probability of wrongly rejecting a given model. The adequation between the different models and the data (as defined by the equation (A2)) is indicated next to the R_u distributions in Figure 6. The values obtained for each model are not small enough to reject one of them with a high enough probability, so that each model is consistent with the observation. Furthermore, the detailed distribution of

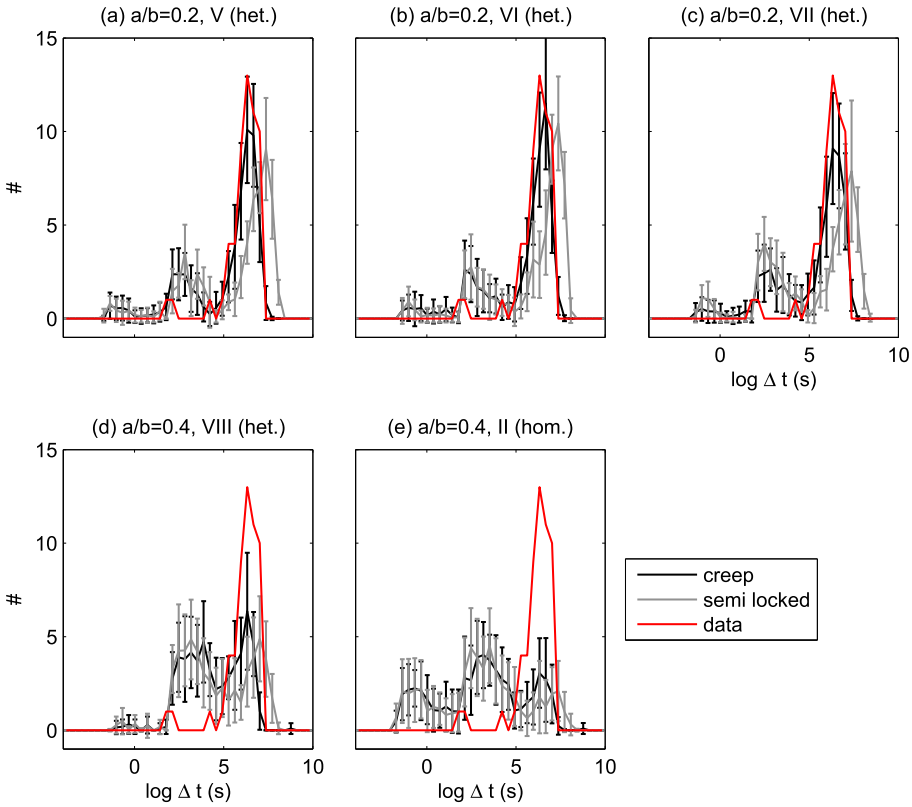

Figure 7. Interevent delay distributions of observed (red) and modeled (levels of gray) sequences. Here again, the modeled sequences are all **Σ** sequences and have been generated by the models highlighted in Table 3. Δt is the time delay in seconds.

the different asperities, and the presence or absence of mechanical heterogeneity within the seismogenic patch does not seem to influence greatly the coseismic slip shape.

However, even if we are not able to reject one model or the other, we note that the coseismic slip distribution is more likely controlled by the overall mechanical conditions (creeping or locked) than by the detailed mechanical structure of the seismogenic patch. This latter issue will be further investigated in section 5 in a more general manner.

4.3.3. Interevent Time Delays

To this point of our study, our results indicate that for both semilocked and creeping conditions, it is possible to find different asperity distributions able to account for the observed (M_{0s}, L_s) scaling and the observed coseismic slip distribution. Furthermore, it has been shown that those asperity distributions have to be characterized by a strong mechanical interaction in order to account for the magnitude range observed. This strong interaction condition could be parametrized by asperities with low a/b values.

The comparison of the interevent time delay distributions (Figure 7) supports to the first order these preliminary conclusions: the multiplet 866 is characterized by a distribution somewhat spread around $T = 23$ days (between 10^5 and 10^7s), which is similar to the distributions produced by the low a/b seismogenic patches, with either creeping or semilocked environment. Once again, assuming larger a/b reduces the similarity with the observations.

However, a more detailed analysis reveals that fully creeping conditions generate sequences with interevent delays closer to what is observed in the multiplet 866, whereas models with semilocked conditions slightly overestimate those delays, especially for $a/b = 0.2$ patches. The maxima of the distributions obtained under semilocked conditions are approximately 10 times larger than the maxima obtained under creeping conditions. Furthermore, the shift between the maxima does not depend on the way asperity are distributed (Figures 7a–7c). The difference in the distributions could therefore be interpreted as the signature of the difference in effective stressing rate felt by the seismogenic patch in models *C* and *SL*. A simple dimensional analysis

developed in Appendix B shows that the characteristic recurrence times for ruptures under semilocked conditions are approximately w/L times larger than what is expected for creeping conditions (equation (B9)). With the parameter used in our simulations, w/L is of the order of 10 which accounts for the shift in the interevent time distributions presented in Figures 7a–7c (between black and gray distributions).

The developments presented in Appendix B also suggest that for a given stressing rate, the interevent delays are proportional to the stress drop of the asperities. If one accounts for the whole possible range of stress drops appearing in Figure 1d (between 1 and 100 MPa), the time delays could vary by 1 order of magnitude. This feature provides an explanation for the scatter in the observed interevent delay distribution. This interpretation of the scatter is, however, questionable, since it could be a consequence of the mechanical interactions among the set of asperities (the rupture of a fault patch could delay or hasten the failure of neighboring asperities). More importantly, because of the uncertainty on the stress drop, the distributions of the modeled interevent delays could be offset by 1 order of magnitude, which is the typical separation between the distribution obtained with creeping and semilocked conditions, making those two models equally able to fit the observed time delays. In other words, a set of asperities characterized by a low stress drop of 1 MPa and surrounded by semilocked conditions could explain the observations as well as a set of stronger asperities entirely surrounded by creep.

Similarly, the ratio between interevent delays under locked and creeping conditions is of the order of $w/h \sim 100$, so that the recurrence times for ruptures within a locked environment would be even larger than what is obtained for semilocked conditions. This would be clearly inconsistent with the observations, even after accounting for the uncertainty in the stress drops. Therefore, even if very particular frictional parameters allowing to generate $\boldsymbol{\Sigma}$ sequences under locked conditions exist, the very low stressing rate on the seismogenic patch under fully locked conditions would hardly explain the high seismicity rate observed.

In addition to the characteristic time of 23 days, we notice that the observations present a small amount of shorter time delays of the order of 100 s, which is also present in our simulations. These small time delays might be due to the interactions leading to some amount of short-term triggering. However, for simplicity this feature will not be discussed any further.

Our results suggest that the multiplet 866 corresponds to a set of coplanar strongly interacting asperities rupturing a small region of a larger fault structure that is at least partly creeping. The main evidence supporting this model is provided by the distributions of estimated stress drops and interevent time delays which imply the presence of a rapidly loading mechanism near the seismogenic patch, such as fault creep. More generally, we showed that the coseismic slip distribution is influenced by the amount of aseismic slip in the vicinity of the asperities, so that it could be used as an indicator of fault creep. In the following section, we investigate in more details this issue for a more general complex multiplet.

5. Coseismic Slip Distribution

Until now, we have shown that the coseismic slip distributions of complex multiplets could provide insights into the mechanical conditions prevailing on the fault segment surrounding the multiplet. This is well illustrated by the results presented in Figure 6 where fully creeping environments generate annular slip distributions, and semilocked conditions generate semiannular slip distributions. Motivated by this result, we analyzed systematically the slip distributions generated in the 30 different models in Table 2 in order to investigate in detail whether the slip distribution is controlled either by the properties of the asperities or by the mechanical environment of the asperities (creeping or locked). In the following, we essentially discuss the two end-member model categories, i.e., the fully creeping models *C* and the fully locked models *L*.

To do so, we construct for each model random $\mathbf{S}$ sequences of n_S successive events according to the definition of $\mathbf{S}$ given in section 4.1, which is without any constraint on the magnitude content. However, the sequences are constructed as before from the modified catalogs, in which undetectable events are removed. Furthermore, we analyze sequences of different sizes n_S.

First, we chose n_S equal to n_0, which is defined in Appendix C as the average number of events releasing a seismic moment equivalent to the rupture of the entire seismogenic patch. Some examples of the coseismic slip distribution shapes obtained for $n_S = n_0$ events are represented in Figures 8 (column 1) and 8 (column 2) for patches made of identical asperities and in Figure 9 for patches with heterogeneous asperities.

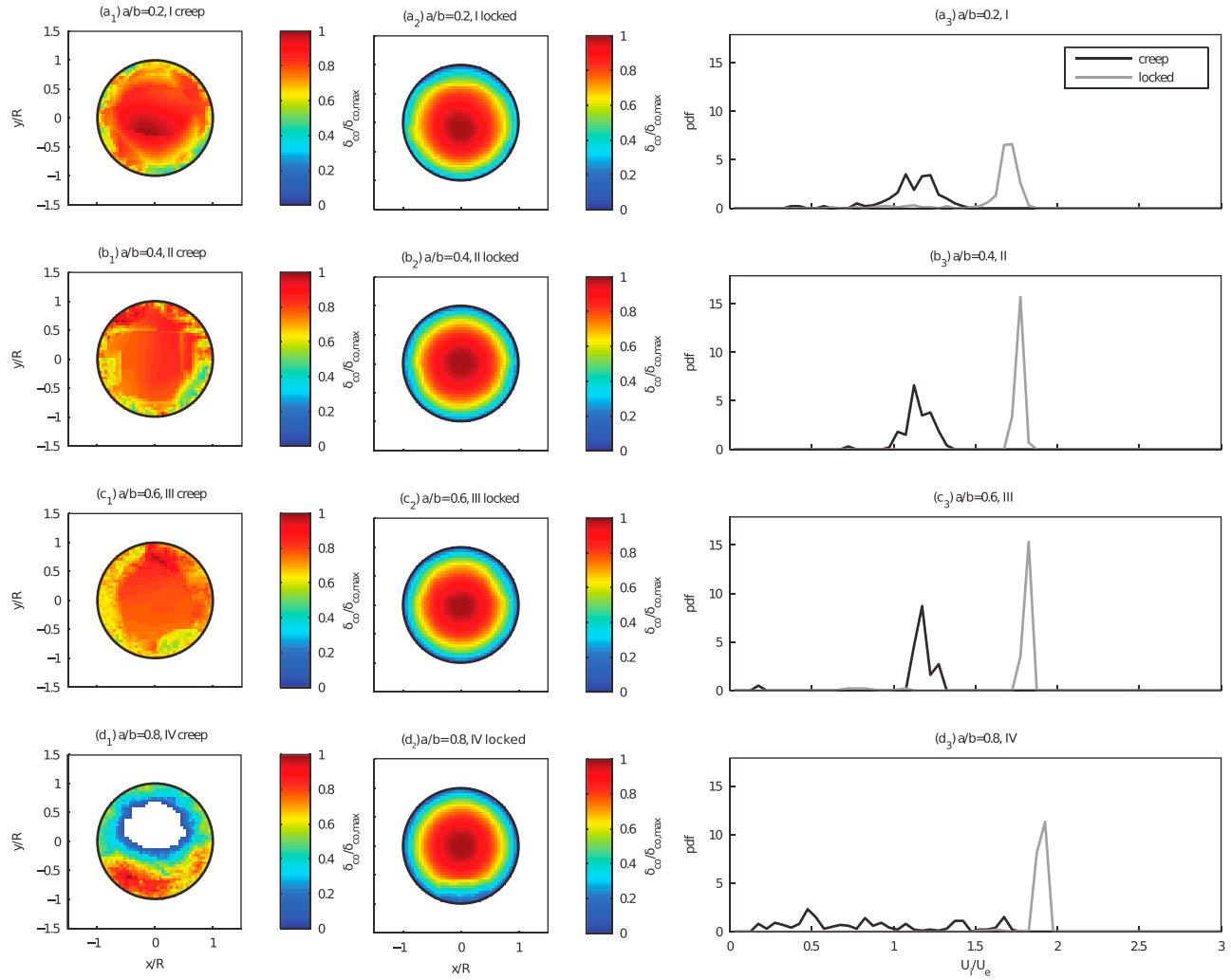

Figure 8. (columns 1 and 2) Comparison between the shape of the cumulative coseismic slip distributions generated by sequences with n_0 events on the seismogenic patch, obtained with overall creeping fault conditions (Figure 8, column 1) and locked conditions (Figure 8, column 2). Here only patches with similar asperities have been considered (structures I to IV in Table 2). The models used are indicated in the title of each subfigure. As defined in equation (C2), n_0 is the average number of events releasing a seismic moment equivalent to the rupture of the entire seismogenic patch. No magnitude criterion has here been used in the selection of the sequences. The color scale indicates the normalized coseismic slip. White areas inside the seismogenic patch did not experience any slip. (column 3) Corresponding distributions of $R_u = U_i/U_e$ parameter. Black lines refer to the results shown in Figure 8 (column 1) and gray lines to the results shown in Figure 8 (column 2).

Note that the coseismic slip δ_{co} has been normalized by its maximum value on the seismogenic patch. The main result arising here is that fully creeping conditions lead to a slip distribution either maximum at the periphery of the patch or roughly uniform over the patch and fully locked conditions lead to a slip distribution maximum at the center of the patch similar to the elliptical slip profile of a crack with constant stress drop [*Eshelby*, 1957]. *Kato* [2009] obtained the same characteristic slip distributions in the case of a single circular asperity.

Furthermore, we notice that the two different slip distributions observed for creeping conditions alternate in time, which once again could be interpreted in terms of nonuniform creep-related stressing rate acting on the seismogenic patch: asperities on the edges of the patch first fail because they are loaded faster than central asperities which accumulate slip deficit. When central asperities have accumulated enough stress, they fail as a big event nucleating in the central part of the seismogenic patch. Before the main event, the slip distribution is larger at the periphery of the patch, but once a large central event occurs, the slip distribution becomes uniform, and another cycle starts.

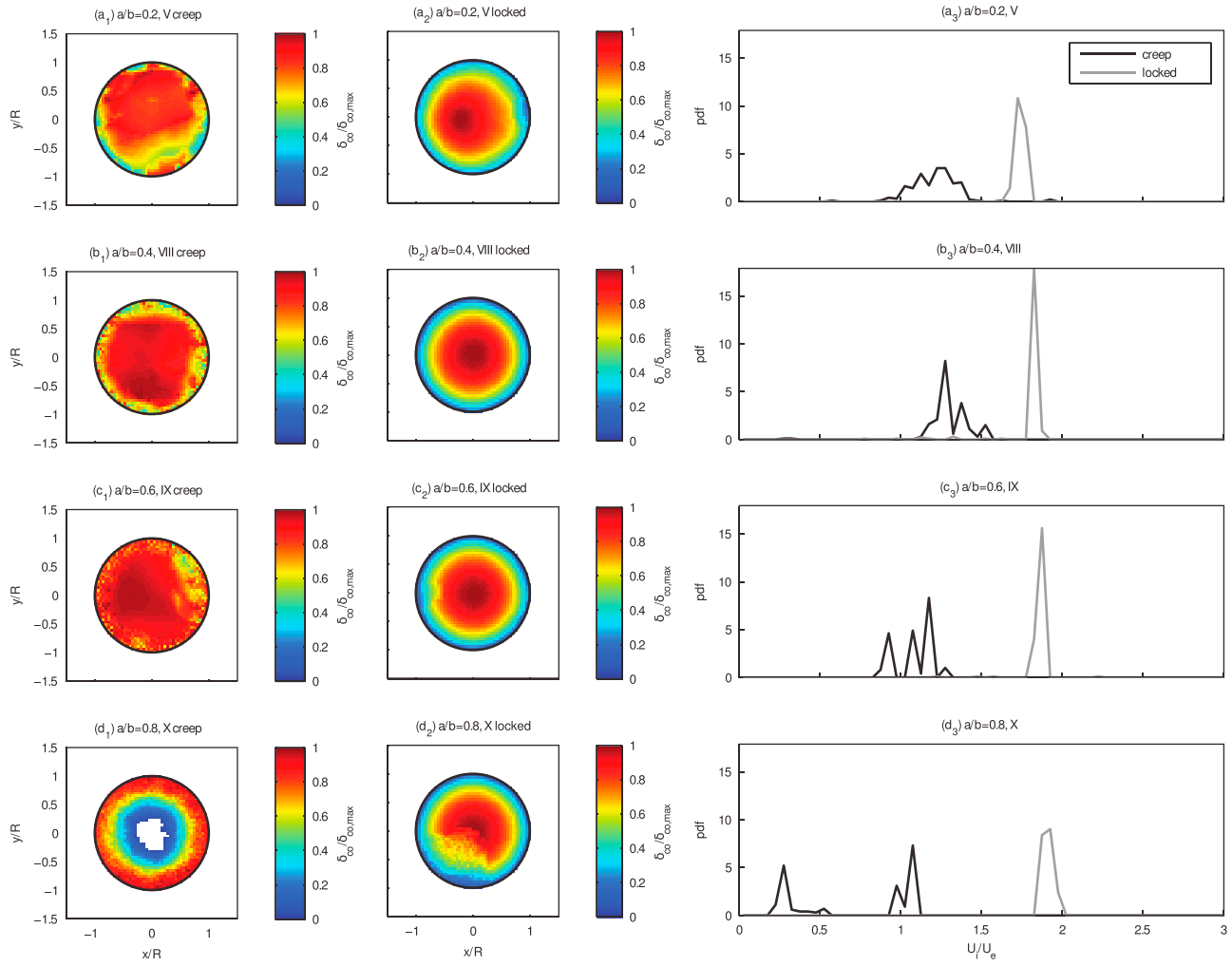

Figure 9. Same diagrams as in Figure 8, for seismogenic patches consisting of a collection of heterogeneous asperities (structures V, VIII, IX, and X in Table 2).

In this framework, the presence of an unbroken area in the center of the seismogenic patch obtained after n_0 events with models IV and X (Figures 8d$_1$ and 9d$_1$) is a consequence of the approximation (C2) of n_0 which is only a rough estimate of the actual number of events releasing a seismic moment equivalent to the rupture of the entire patch. This issue will be further discussed later when analyzing the evolution of the R_u distribution with n_S. The limits of equation (C2) is also visible in the small deviation from symmetry appearing in the slip distributions in Figures 8 and 9, especially with the patch model *X*. Even when asperities are identical, from our modeling assumption they rupture independently, and the symmetric simple organization of the cumulative slip requires a sufficient number of events to occur.

The most important result here concerns the R_u distributions represented in Figures 8 (column 3) and 9 (column 3). These diagrams indicate that the cumulative slip distributions are rather stable in time, each R_u distribution being the result of an analysis of 200 **S** sequences for one catalog. When the fault region surrounding the patch region is locked, the R_u distribution tends to a delta function centered on a value between 1.5 and 2. As a comparison, the R_u value expected for an elliptical slip distribution is $8/\sqrt{3} - 3 \sim 1.61$, which is within the range of our numerical results. In contrast, R_u distributions for fully creeping environments are limited between 1 and 1.5, at least for $a/b < 0.8$, 1 being the R_u value expected for a uniform distribution of slip. For some models (in particular for the patch structure *X*), the R_u distribution associated with fully creeping conditions is bimodal, exhibiting as previously a maximum between $R_u = 1$ and $R_u = 1.5$ as well as a maximum for $R_u < 0.5$. This latter small value of R_u is expected when the slip distribution is maximum at the periphery of the model.

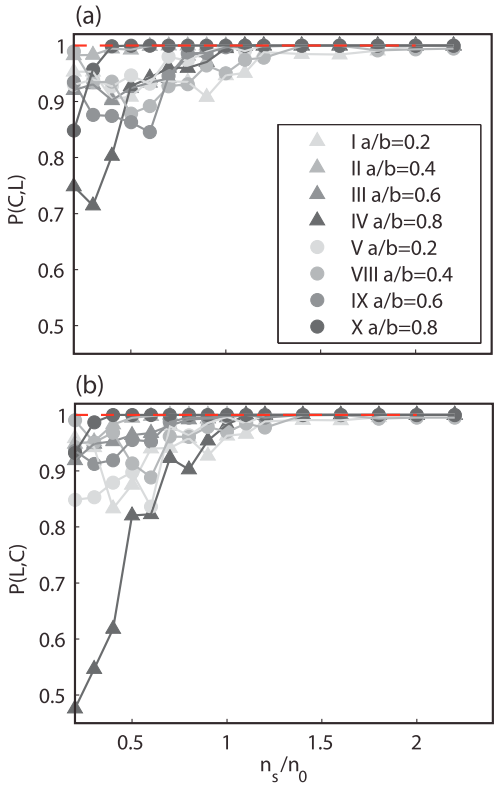

Figure 10. Separability of creep and locked models C and L for different patch structures indicated in Table 2, as a function of the normalized number of observed events n_S/n_0. The number of events within a sequence is n_S, and n_0 is the estimate defined in equation (C2) of the average number of events releasing a seismic moment equivalent to the rupture of the entire seismogenic patch. (a) Separability defined as the probability $P(C, L)$ given in equation (15). (b) Separability defined as the probability $P(L, C)$ given in equation (14). When $P(C, L)$ (or $P(L, C)$) is sufficiently close to unity, it corresponds to the probability of properly rejecting model L (or C) when compared to data generated by model C (or L). The different levels of gray correspond to different values of the a/b ratio. Triangles correspond to models with identical asperities and circles to models with heterogeneous asperities. The dashed red line indicates a probability of 1.

An important point to notice here is that the slip distribution shape is mostly controlled by the mechanical environment of the seismogenic patch (locked or creeping) and not by the properties of the asperities within the seismogenic patch. The slip distributions obtained for locked conditions are indeed nearly identical if we consider different a/b ratios or different degrees of mechanical heterogeneity between the asperities. We also ensured that the slip distribution does not either depend on the detailed distribution of the asperities, in the sense that seismogenic patches V–VII produce the same results. Similar results are obtained with different patches because the number of events in one sequence is high enough so that the probability of rupturing the entire patch area during one sequence is high. For a smaller number of events (i.e., smaller than n_0), some asperities may not rupture, which is typically the case of the $\mathbf{\Sigma}$ sequences used in the previous section. The particular R_u distribution generated by the seismogenic patch X under creeping conditions (Figure $9d_3$) could be interpreted in the same manner: n_0 events are not sufficient in this case to break the entire patch area.

To that point, different fault environments generate very distinct slip distributions on the seismogenic patch, and thus very distinct R_u distributions. R_u distribution could therefore be used as an indicator of the presence of creep or locked patches in the vicinity of the sources. However, such a method requires that a sufficient number of events have occurred on the seismogenic patch. In the following, we estimate the minimum number of observed events necessary to make R_u distributions distinct enough. For that, we compute for each model the R_u distribution for different sequence sizes n_S, and we estimate the separability of the distributions generated with fully creeping and fully locked conditions according to the method described in Appendix A. Recall that this method allows to estimate the probability of properly rejecting a model m_2 (considered as a null hypothesis) in the case the model m_1 is correct (i.e., producing the analyzed data). For each seismogenic patch, we successively assumed the creep model C and the locked model L as the reference model m_2. In this framework, the probability $P(L, C)$ of properly rejecting the creep model (considered as the null hypothesis) if the locked model is the correct one is given by

$$P(L, C) = 1 - \Pi_{L,C}, \tag{14}$$

where $\Pi_{L,C}$ is defined in Appendix A. As mentioned in Appendix A, $P(L, C)$ could only be interpreted as a probability if it is sufficiently close to one. Similarly, the probability $P(C, L)$ of properly rejecting the locked model if the creep model is the correct one is given by

$$P(C, L) = 1 - \Pi_{C,L}. \tag{15}$$

Here we use $P(L, C)$ and $P(C, L)$ as two different estimates of the separability of the R_u distributions. The evolution of $P(L, C)$ and $P(C, L)$ as a function of n_S are represented in Figure 10. For $n_S/n_0 \geq 1$, if one of the two different models is correct, the other model could be rejected at more than the 95% confidence level. In other words, as soon as the number of observed events exceeds n_0, the distribution of the cumulative coseismic slip generated by a complex multiplet is a good indicator of the presence of creep or locked patches in the vicinity of the microearthquakes source region. For a smaller number of events, the separability could still be good, depending on the properties of the asperities. As shown in Figure 10, sequences generated by weakly interacting asperities (with high a/b) are characterized by a very low separability (down to 0.4) when n_S is much smaller than n_0, whereas in the case of strongly interacting asperities, the separability is still larger than 0.8 for $n_S = 0.2n_0$.

6. Discussion

The set of simulations analyzed here provides insights into the seismic behavior of a small set of coplanar asperities embedded in a larger fault region. Such a modeling approach allows to interpret the mechanical environment in which a microseismic multiplet is active, in particular if this environment undergoes aseismic creep at a larger scale or not. This predictive potential has been tested in two different contexts: first by modeling the source region of the multiplet 866 and then in a more general microseismic source context.

6.1. Multiplet 866

Our main conclusion concerning the multiplet 866 is that it could hardly be interpreted as a set of asperities surrounded by a locked fault environment. This conclusion is first supported by our simulations with locked fault conditions showing a very specific swarm-like pattern very sensitive to the friction on the patch (a and b parameters). None of the swarms produced contained sequences with a similar magnitude content than observed ($\mathbf{\Sigma}$ sequences). Obtaining a $\mathbf{\Sigma}$ sequence on a locked fault would require a very specific asperity distribution that we were not able to determine. This issue could be addressed, for instance, by identifying the parameters controlling the development of such swarms, which is well beyond the scope of this study. More importantly, this regular pattern of swarms is never observed for creeping environment. Recently, *Kato* [2014] reported a similar feature: their simulations showed important differences in the regularity of failures occurring on a single asperity, depending on its locked or creeping surroundings. Aperiodicity of the ruptures, for instance, could only be obtained in a creeping environment, not in a locked environment. This could be interpreted as complex stress transfers between creep and asperities. This difference could constitute an interesting element allowing to discriminate between locked and creeping environments, as the slip pattern does. However, such a method requires to observe multiplets over a much longer time period. Here again this issue has to be further investigated.

In our modeling of the multiplet 866, the seismicity pattern is controlled not only by the overall fault environment (creeping or locked) but also by the properties of the asperities, which extends the conclusions of several studies about discrete models of faults [*Rice*, 1993; *Rice and Ben-Zion*, 1996; *Ziv*, 2003; *Ziv and Rubin*, 2003; *Ziv and Cochard*, 2006]. However, we noticed that for a given population of heterogeneous asperities, the detailed spatial organization had a smaller influence on the seismicity pattern than some average frictional parameters, such as the ratio a/b or the extreme values of the $a - b$ parameter. This dependence is true not only for locked fault environments (a and b sensitive swarms) but also for creeping environments, since all the patch structures tested with aseismic surroundings were not equally able to fit the observations. In particular, frictional properties enhancing the growth of seismic ruptures, such as low a/b ratios, are necessary to generate the correct magnitude-frequency distribution. Moreover, the use of heterogeneous seismogenic patches increased the complexity in time and magnitude range. However, the influence of the properties of asperities on the pattern of seismicity was reduced by the presence of surrounding creep, as shown by the larger range of seismogenic patches able to fit the observations when creeping conditions prevail.

To this point, it is important to mention that $a/b = 0.2$ is much below what is usually suggested by laboratory measurements, and $b - a = 0.015$ lies in the very upper limit of what is observed [*Marone*, 1998]. This discrepancy could possibly support the assumption that rate-and-state parameters are extremely different in natural and laboratory conditions. An alternative explanation would be that a model involving very small a/b values is equivalent (in terms of asperity interaction) to a more realistic model with large a/b, but with an heterogeneity of the critical slip d_c. d_c indeed plays a role in the mechanical interactions between the sources because the response of an asperity to an external stress perturbation involves an acceleration of slip

over a timescale approximately given by $t_0 = ad_c/bv_0$ in the case of the aging version of the state evolution law, where v_0 is the instantaneously perturbed sliding velocity [*Perfettini and Ampuero*, 2008]. Thus, smaller d_c make asperities more sensitive to neighboring failures and increase the probability of such asperities to be involved in larger ruptures [*Hillers et al.*, 2006]. The scatter in magnitudes could therefore be explained in terms of heterogeneities in d_c over the seismogenic patch.

In the case of the multiplet 866 the main piece of evidence arguing against a locked fault environment comes from the average seismicity rate (or more specifically the distribution of interevent time delays) and the observed stress drops that require the presence of a nearby loading mechanism. Such a loading mechanism could be a creeping zone slipping at the opening rate of the rift but could also be driven by overpressurized fluids, which may play a significant role in the activation of microseismic swarms within the gulf [*Bourouis and Cornet*, 2009]. However, the pressure increase would have to activate asperities at a rate of the order of 1.5 cm/yr. Extending updip the creep inferred for the detachment zone from geodetic observations constitute a much simpler mechanical model.

Moreover, in our simulations, the distribution of interevent delays could be influenced by the different thresholds used to eliminate undetectable events of the catalog, such as the minimum observable magnitude m, and the minimum time delay between separable events $\Delta t_{\min} = 100$ s. These thresholds mainly influence the number of small events and the content of the 56 events samples. Because time delays larger than 100 s are observed in the multiplet 866, it is assumed here that $\Delta t_{\min}$ could only be lower than 100 s. Decreasing $\Delta t_{\min}$ while keeping the number of events within one sequence constant enhances the ratio between small (i.e., smaller than $\Delta t_{\min}$) and large time delays. However, large time delays could only be modified by ± 100 s which is negligible compared to the average time delay of 23 days. Hence, the position of the maxima of the modeled distributions presented in Figures 7 are not modified when lowering $\Delta t_{\min}$, even if their amplitude is reduced. Even larger time delays expected for locked conditions would also not be significantly modified. Therefore, our conclusion that locked conditions would probably not produce time delays of the order of 23 days is not affected by our choice of $\Delta t_{\min}$. The effect of changing the minimum observable magnitude m is more difficult to estimate, because it depends on the way small events cluster in time relative to the larger events. If smaller events only participate in rapid aftershock sequences, one could expect time delays smaller than $\Delta t_{\min}$ so that the distribution at larger time delays is not significantly affected by m. Consequences might be more important for an uncorrelated seismicity generated by heterogeneous sets of asperities. Our synthetic sequences generate a larger amount of small-magnitude earthquakes (i.e., smaller than 1.4) than observed in the multiplet 866. To explain this, we suggested a completeness magnitude for the observed seismicity of the order of 1.4. Therefore, m could be considered between 0.9 and 1.4, and we tested these different values, but no significant consequence on the time delay distributions was observed.

Furthermore, we noticed that changing $\Delta t_{\min}$ or m did not generate Σ sequences within locked environments, first because it did not increase the number of small events enough for that and then because it had no influence on the content of intermediate events (of the order of $M_w = 2$) which are accounted for in the construction of Σ sequences. Finally, changing the ratio between small and intermediate magnitude events did not affect significantly neither the slip amplitude and slip distributions nor the (M_{0s}, L_s) scaling.

6.2. Implications for Seismic Hazard in Corinth

The multiplet 866 being situated on the edge of the rupture area of the M_w6.2 Aigion earthquake [*Lambotte et al.*, 2014; *Godano et al.*, 2014], our results would imply that the fault segment activated by the 1995 main shock is at least partly creeping. Recall that the multiplet 866 only attests for creep during the 7 years period between 2001 and 2007: data being only available for this specific time period.

Because of the uncertainty on the stress drop estimation (between 1 and 100 MPa), both a creeping and a semilocked model could be proposed for this area (Figure 2). This result constrains the western limit of a potentially larger scale locked asperity on the multiplet itself. A model assuming aseismic creep to the west of the multiplet 866 and a locked region to the east is supported by the aftershocks distribution of the 1995 earthquake. As shown by *Bernard et al.* [1997], the aftershock activity was mainly located to the west of the multiplet 866 and could be interpreted as the failure of smaller asperities embedded in a creeping region activated by the main shock. Such an aftershock mechanism driven by aseismic creep is supported by the studies of *Schaff et al.* [1998] or *Bourouis and Bernard* [2007] for creep coupled with pore pressure migration. The same pattern of higher seismicity to the west of the rift is also typical of the background activity in this region between 2000 and 2007 [*Lambotte et al.*, 2014].

As an alternative model, it would be possible to interpret this multiplet as a nucleation process that will degenerate in a larger instability. This model is suggested by our simulation results showing usually a maximum event of the order of $M_w = 4$, sometimes preceded by an accelerating seismic activity, in particular for locked fault conditions. In other words, some of the synthetic Σ sequences belong to a nucleation process of a larger earthquake, which could occur as a localization and acceleration of slip on a small patch of constant length [*Dieterich*, 1992; *Rubin and Ampuero*, 2005; *Ampuero and Rubin*, 2008]. Furthermore, *Bouchon et al.* [2013] reported acceleration of seismicity possibly associated with such large nucleation phases. In this framework, an important point to address would be whether the nucleation process could lead to an event of magnitude much larger than 4, which is an event destabilizing the seismogenic patch and the creeping segments around it. A major destabilization of a creep and asperity system such as the one observed in Corinth might occur if the local density of asperities exceeds a critical value [*Dublanchet et al.*, 2013a]. Elevated pore pressure conditions suggested by *Bourouis and Cornet* [2009] could, for instance, lower this critical density of asperities and promote major ruptures.

As repeating earthquakes do, complex multiplet sequences provide insights on the local deformation of fault zones. The approach used here could in particular be extended to other multiplets in the Corinth area and motivates further studies. However, the multiplet considered here has been chosen because of its isolated location, its nearly planar structure, and its particular position relative to the seismic stations in the gulf, which is not the case of all multiplets in the Corinth area.

6.3. Complex Multiplets as Creep Meters

A more general question arising from our analysis of the multiplet 866 is whether coseismic slip generated by a complex multiplet could be used as a measure of the local creep rate at depth. Here it has been shown that slip on the seismogenic asperities does not necessarily imply creep in the vicinity, as this is usually assumed for repeating earthquakes. The source region could be a weaker patch within a stronger locked fault region, loaded by a remote mechanism. In order to estimate a local creep rate, it is first necessary to assess the occurrence of aseismic creep in the vicinity of the earthquake sources, and we have shown that the most robust way to identify it is to monitor the shape of the cumulative coseismic slip generated by a sufficient number of events. It turned out that in the case of the multiplet 866, we could not find a way to produce realistic sequences without the presence of creep so that the analysis of cumulative coseismic slip distribution was not critical. However, the simulations performed in section 5 showed that in a more general case, the creep control of the cumulative coseismic slip shape is a robust feature one could rely on.

Once the presence of creep is attested, it becomes possible to compare the slip accumulated on the microseismic source region and the amount of creep in the surrounding region over a similar time period. As shown for the multiplet 866, the stressing rate acting on the source region could be roughly estimated from the stress drops and the distribution of interevent time delays, assuming that the seismicity rate is proportional to the stressing rate. This assumption is usually true for noninteracting rate-and-state sources as long as the characteristic duration of aftershock sequences is small compared to the timescale of stress variation [*Dieterich*, 1994; *Helmstetter and Shaw*, 2009]. *Ziv and Rubin* [2003] extended this result to interacting sources showing that the seismicity rate is still proportional to the stressing rate in this context. However, only a rough estimate is possible with such assumption because of the uncertainty on the patch structure and on the stress drops (between 1 and 100 MPa in the case of the multiplet 866).

Moreover, the coseismic component of slip on the source region derived from seismic data is only an underestimation of the total slip accumulated that could be partly aseismic. The occurrence of an aseismic component of slip on asperities has been suggested by *Chen and Lapusta* [2009] in order to explain the scaling between seismic moment and recurrence time of repeating earthquakes. Their asperity model reproduced the observed scaling because the seismogenic asperities embedded in a creeping area accumulated a significant fraction of aseismic slip, in particular when they were close to their critical size. This aseismic slip occurred during the interseismic period, as a penetration of surrounding aseismic slip within the asperities. In our simulations, we estimated the fraction of aseismically released slip on the asperities only in the case of the locked fault environment, and in these conditions, it only represented less than 1% of the total accumulated slip. We expect a similar result for creeping environments, because the surrounding aseismic slip could only penetrate at a distance of the order of the critical length for nucleation [*Chen and Lapusta*, 2009], which is smaller than the asperity size assumed here. In other words, only the most external asperities of the seismogenic patch would accumulate aseismic slip, which is a small fraction of the total patch area. The coseismic

slip inferred for the multiplet 866 (of the order of 10 cm) is therefore a good estimate of the total slip. However, a better estimation would require a more detailed study of the parameters controlling the proportion of aseismic slip in a multiple asperity context.

Similarly, the total slip accumulated by the source region might be underestimated because undetectable events could be missing. The fraction of total slip accumulated by this category of events in our catalogs was in each model 1 order of magnitude smaller than the fraction of aseismic slip, which is less than 0.01%. However, the contribution of small events in our models depends on the thresholds used to eliminate undetectable events and on the minimum asperity size assumed. Estimating the contribution of undetected events in the case of natural seismicity similarly depends on the detection threshold of the network, the processing techniques, and on the minimum possible rupture size. Note that in our modeling approach of the multiplet 866, the minimum asperity size was determined from the minimum observed source size and therefore does not necessarily represent the actual minimum source size in the multiplet, which could be much smaller. The actual small events contribution might therefore be much more important than 0.01%.

From a systematic study of slip distributions, we conclude that a cluster of coplanar asperities remotely loaded behave in an organized manner as soon as a critical number of events have occurred. In other words, when averaged over a large enough number of events, the mechanical behavior of the asperities does not depend any more on the detail of the properties of the asperities, but on the general mechanical conditions in which these asperities are active (i.e., a locked or a creeping fault). The minimum number of events n_0 required to get such an organized average response is approximately given by the number of events necessary to release the seismic moment of the largest possible event (i.e., the event rupturing the entire cluster of asperities as a whole). We notice here that n_0 could vary, for the same patch size and the same number of asperities over several orders of magnitudes, from 2 in the case of strongly interacting asperities (characterized, for instance, by $a/b = 0.2$), up to 20,000 in the case of independent asperities (characterized, for instance, by $a/b = 0.8$). n_0 is thus friction dependent.

For a given observed sequence, the ratio between the number of observed events n_S and n_0 could be estimated from the developments presented in Appendix C. In the case of the multiplet 866, for instance, if we assume that the area covered by the ruptures is stable in time, the size of the seismogenic patch R is approximately given by $R^* = 350$ m. Furthermore, from Figure 1d, the stress drop $\Delta\tau$ is between 1 and 100 MPa, and from Figure 1c, the cumulative coseismic moment is $M_S = 5.10^{13}$ N m. We finally obtain after using the equation (C6) a ratio n_S/n_0 between 0.005 (for $\Delta\tau = 100$ MPa) and 0.5 (for $\Delta\tau = 1$ MPa). If a particular asperity distribution is able to generate $\boldsymbol{\Sigma}$ sequences under locked fault conditions, the results presented in Figure 10 can help to estimate the separability between the locked and creeping models. Furthermore, we note that in the case $n_S/n_0 = 0.5$, doubling the number of observations by analyzing data between 2007 and 2015 would increase the separability from 0.8 to at least 0.95. More generally, the monitoring of seismic moment and slip distribution on a complex multiplet provide enough tools to estimate the probability that creep and locked models are suitable.

7. Conclusion

A mechanical model comprising a wide range of frictional behaviors allows to interpret complex sequences of coplanar microseismicity clusters in terms of fault mechanical properties. In particular, we have demonstrated that the seismicity rate and the coseismic slip of a cluster of asperities are strongly influenced by the mechanical behavior of the fault area that surrounds it. If the asperities are located on a locked fault segment, the coseismic displacement tends to be concentrated at the center of the cluster, whereas it is more uniform if the cluster lies on a creeping fault. Similar modeling approaches could be implemented systematically for all the complex microseismic sequences of a given active region and could improve the understanding of fault behavior beyond the constraints provided by the simplest regular sequences. Mechanical modeling of microseismic sources as presented in this study is of fundamental importance because it allows to infer aseismic deformation at depth from seismic data, without relying on geodetic measurements.

Appendix A: Adequation Model Data and Separability of Models

Let x be a random variable representing the data, either observed or synthetic (predicted by a model m). We define the probability density $\rho_d(x)$ of the data, related to the uncertainties of the outcome of measurements,

and $\rho_m(x)$ the probability density of the prediction of a model m, equivalent to the a priori probability density of x assuming m is true (null hypothesis). Let $\Pi(x, m)$ be the proportion of subsets of the data space, x', for which $\rho_m(x') < \rho_m(x)$. We have

$$\Pi(x, m) = \int_{x';\rho_m(x')<\rho_m(x)} \rho_m(x')\mathrm{d}x'. \tag{A1}$$

When observing a single value x_d, with no uncertainties ($\rho_d(x) = \delta(x - x_d)$), getting a small values of $\Pi(x_d, m)$ allows to reject model m if this value is smaller than a predefined level Π_0. For instance, taking $\Pi_0 = 0.01$ for a Gaussian distribution allows to reject the model at 3 standard deviations; i.e., with a probability smaller than 0.01 to wrongly reject the null hypothesis of model m. When dealing with a more general distribution of the data $\rho_d(x)$ (set of independent measurements, or single measurement with uncertainties), one can define

$$\Pi_{d,m} = \int \rho_d(x)\Pi(x, m)\mathrm{d}x, \tag{A2}$$

and for $\Pi_{d,m}$ sufficiently small, one can again reject the model m with a probability $\Pi_{d,m}$ to be wrong. In the main text, we define $\Pi_{d,m}$ as the adequation between the model and the data.

This formulation also allows to compare the predictions of two competing models m_1 and m_2. We calculate $\Pi_{d,m1}$ and $\Pi_{d,m2}$, and set a rejection threshold Π_0. The domains for which two, one, or none of the models are rejected define their relative resolution and their separability in the data space. This can be quantified by calculating $\Pi_{d,m1}$ (null hypothesis m_1) assuming that d is in fact produced by model 2 (i.e., $\rho_d(x) = \rho_{m2}(x)$). When sufficiently small ($<\Pi_0$), the resulting $\Pi_{m2,m1}$ can be taken as the probability that the model 1 (null hypothesis) would not be rejected if model 2 is true.

In section 5, $\Pi_{m2,m1}$ is used to evaluate the separability of seismogenic patch models assuming creeping or locked fault conditions. We therefore define $\Pi_{C,L}$ as the probability of wrongly rejecting a model with locked conditions if a model with creep conditions is true. Similarly, $\Pi_{L,C}$ is the probability of wrongly rejecting a model with creep conditions if a model with locked conditions is true.

Appendix B: Interevent Time Delays

In this section an approximation for the time delay between successive ruptures within the seismogenic patch of Figure 3 is derived. The development presented here is based on the assumption that for a single asperity, the recurrence time for ruptures T_{asp} is approximately given by the ratio between the stress drop $\Delta\tau$ and the stressing rate $\dot{\tau}$:

$$T_a \sim \frac{\Delta\tau}{\dot{\tau}}. \tag{B1}$$

For simplicity, we assume that the seismogenic patch is made of a population of n_{asp}-independent asperities rupturing in an uncorrelated manner, with the same stress drop $\Delta\tau$. In these conditions, the recurrence rate of ruptures T within the patch is approximately given by $T_{\mathrm{asp}}/n_{\mathrm{asp}}$. After using equation (B1), we end up with

$$T \sim \frac{\Delta\tau}{n_{\mathrm{asp}}\dot{\tau}}. \tag{B2}$$

The assumption of proportionality between average seismicity rate and stressing rate is supported by *Dieterich* [1994], *Ziv and Rubin* [2003], and *Helmstetter and Shaw* [2009].

In this framework, the main consequence of changing the fault environment from creeping to locked conditions is to modify the stressing rate acting on the asperities. In order to quantify this effect, we first remark that the stressing rate $\dot{\tau}$ is the sum of two different terms: the stressing rate associated with the remote tectonic loading $\dot{\tau}_{\mathrm{tect}}$, and the stressing rate associated with the surrounding creep $\dot{\tau}_{\mathrm{creep}}$. From equation (2), $\dot{\tau}_{\mathrm{tect}}$ is of the order of $\mu v_p/w$, where μ is the shear modulus, v_p the remote loading rate, and w the distance from the tectonic loading source. Similarly, an order of magnitude for $\dot{\tau}_{\mathrm{creep}}$ is given by $\mu v_c/h$, where v_c is an order of magnitude of the creep rate on the fault segment surrounding the seismogenic patch and h is the asperity size, which is an estimate of the minimum distance to creep regions. Here v_c is different for creeping and semilocked conditions.

For creeping conditions first, the average long-term slip on every point of the fault (and in particular on the creeping regions) follows the tectonic loading, so that v_c is of the order of v_p. However, for semilocked conditions, v_c could be approximated as follows: let assume that half of the fault plane of length L presented in Figure 3a is creeping, the other half being constrained against any slip. Because the equivalent mechanical model 3a is periodic in x and y direction [see *Dublanchet et al.*, 2013a], the creeping segment of the fault lies between two locked patches separated by a distance $L/2$, so that the characteristic stiffness k of the creeping segment, for a given shear modulus μ is of the order of $k \sim 2\mu/L$. Furthermore, slip is forced on this segment by a remote slip acting at a distance w. The creeping segment could therefore be modeled as a block connected to a fixed point through a spring of stiffness k on one side, and to a point moving at the tectonic loading rate v_p through a spring of stiffness $k_t = \mu/w$ on the other side. At steady state, the block (i.e., the creeping segment) is moving at a constant velocity v_c, which could be obtained from a force balance on the block itself. This equilibrium could be written as

$$k_t(v_p - v_c) = kv_c, \tag{B3}$$

so that we end up with

$$v_c = \frac{1}{1 + k/k_t} v_p = \frac{1}{1 + 2w/L} v_p, \tag{B4}$$

and assuming $w >> L$ as in the system considered in this study, we get the following approximation:

$$v_c \sim \frac{L}{2w} v_p. \tag{B5}$$

We end up with the following approximation of the total stressing rates $\dot{\tau}_C$ and $\dot{\tau}_{SL}$ in the fully creeping and semilocked conditions, respectively,

$$\begin{cases} \dot{\tau}_C \sim \dot{\tau}_{\text{tect}} + \dot{\tau}_{\text{creep}} \sim \dfrac{\mu v_p}{w} + \dfrac{\mu v_p}{h} \sim \dfrac{\mu v_p}{h} \\ \dot{\tau}_{SL} \sim \dot{\tau}_{\text{tect}} + \dot{\tau}_{\text{creep}} \sim \dfrac{\mu v_p}{w} + \dfrac{\mu L v_p}{2wh} \sim \dfrac{\mu L v_p}{2wh}, \end{cases} \tag{B6}$$

where the last simplification accounts for $w >> L >> 2h$. This allows to rewrite the estimate (B2) of the mean interevent delays T_c and T_{SL} obtained with creeping and semilocked conditions as

$$\begin{cases} T_C \sim \dfrac{\Delta\tau h}{n_{\text{asp}} \mu v_p} \\ T_{SL} \sim \dfrac{2\Delta\tau wh}{n_{\text{asp}} \mu L v_p}. \end{cases} \tag{B7}$$

With the same kind of approach, the characteristic recurrence time in the case of fully locked conditions T_L could be obtained simply by considering the remote tectonic loading as the principal source of stress so that we get

$$T_L \sim \frac{\Delta\tau w}{n_{\text{asp}} \mu v_p}. \tag{B8}$$

From the expression of T_C, T_{SL}, and T_L, we get the following ratios:

$$\begin{cases} \dfrac{T_L}{T_C} \sim \dfrac{w}{h} \\ \dfrac{T_{SL}}{T_C} \sim \dfrac{2w}{L}. \end{cases} \tag{B9}$$

To this point, it is important to insist that this formulation is only valid in the case of a population of isolated uncorrelated asperities, which is different from the population of interacting asperities considered here,

although some of them (the weakest one) might behave in an independent manner. The problem of finding the distribution of time delays within a set of different interacting asperities requires more investigation, which is well beyond the scope of this study.

Appendix C: Average Number of Events Releasing the Total Seismic Moment of the Seismogenic Patch

Lets assume a circular seismogenic patch made of a collection of asperities as depicted in Figures 2 and 3. This patch of radius R would release a seismic moment M_R when rupturing as a whole, which is when all the asperities fail together in a single event. However, when this patch is mechanically loaded, all the asperities do not always fail together and the seismic activity occurs as a sequence of n_{tot} events with different magnitudes (Figure 4). Consequently, more than one event are needed to break the entire area of the patch. In this section, we derive the estimate n_0 for this number of events. To do that, we first notice that the sequence of n_{tot} events releases as much seismic moment as a sequence of n_R identical events of seismic moment M_R, if n_R is given by

$$n_R = \frac{M_{\text{tot}}}{M_R}, \tag{C1}$$

where M_{tot} is the total seismic moment released by the n_{tot} events of the sequence. Therefore, the equivalent number of entire patch ruptures in the original sequence is n_R. Since n_0 events have to release a total seismic moment M_R, n_0 is simply given by the ratio between the total number of events in the sequence n_{tot} and the number of entire patch ruptures in the sequence n_R, so that we get, after using equation (C1)

$$n_0 = \frac{M_R}{M_{\text{tot}}} n_{\text{tot}}. \tag{C2}$$

With the definition (C2), if the seismogenic patch always ruptures as a whole, we obtain $n_0 = 1$. Otherwise, $n_0 > 1$. The ratio between the number of observed events n_S and n_0 is given by

$$\frac{n_S}{n_0} = \frac{M_{\text{tot}}}{M_R} \frac{n_S}{n_{\text{tot}}}. \tag{C3}$$

In Figures 8–10, n_S/n_0 is computed for our synthetic sequences. n_{tot} and M_{tot} are directly provided by the synthetic catalogs as the total number of simulated events end the total seismic moment released during the entire simulation, after removing the undetectable events. The number of events observed in a **S** sequence is n_S. M_R is more difficult to obtain. However, in all our simulations, we noticed at least one occurrence of an event rupturing the entire seismogenic patch, which was generally the maximum magnitude event in the synthetic catalog. Therefore, M_R was computed as the seismic moment released by the maximum magnitude event of the entire sequence (usually $M_w = 4$). Note that $M_w = 4$ is the magnitude expected for a rupture size $R = 320$ m with approximately 10 MPa stress drop, from equations (7) and (13).

In the case no event ruptures the entire seismogenic patch, M_R could be approximated assuming that all the asperities are characterized by the same stress drop $\Delta\tau$. From *Madariaga* [1979], M_R is in this case given by

$$M_R = \frac{16}{7} \Delta\tau R^3, \tag{C4}$$

so that we have

$$\frac{n_S}{n_0} = \frac{7M_{\text{tot}}}{16\Delta\tau R^3} \frac{n_S}{n_{\text{tot}}}. \tag{C5}$$

Finally, if the entire sequence is observed, we have $n_S = n_{\text{tot}}$, the equation (C5) simplifies to

$$\frac{n_S}{n_0} = \frac{7M_{\text{tot}}}{16\Delta\tau R^3}. \tag{C6}$$

This alternative formulation allows to estimate the ratio n_S/n_0 for a natural sequence, provided the source parameters (seismic moments and stress drops) and the size R of the seismogenic patch are estimated independently.

Acknowledgments
We thank the anonymous reviewers and the Associate Editor for all their comments that greatly improved the original manuscript. The authors benefited from the support of the Swiss Seismological Service of ETH Zürich, the Seismological Laboratory of the IPG Paris, and from a CNRS funding. All the simulation results and the numerical model used in this study are available on request to the first author (pierre.dublanchet@sed.ethz.ch).

References

Ampuero, J., and A. Rubin (2008), Earthquake nucleation on rate and state faults: Aging and slip laws, *J. Geophys. Res.*, *113*, doi:10.1029/2007JB005082.

Beeler, N., D. Lockner, and S. Hickman (2001), A simple stick-slip and creep-slip model for repeating earthquakes and its implication for microearthquakes at Parkfield, *Bull. Seismol. Soc. Am.*, *91*(6), 1797–1804.

Bernard, P., et al. (1997), The $M_S = 6.2$, June 15, 1995 Aigion earthquake (Greece): Evidence for low angle normal faulting in the Corinth rift, *J. Seismol.*, *1*, 131–150.

Bernard, P., et al. (2006), Seismicity, deformation and seismic hazard in the western rift of corinth: New insights from the Corinth Rift Laboratory (CRL), *Tectonophysics*, *426*, 7–30.

Bouchon, M., V. Durand, D. Marsan, H. Karabulut, and J. Schmittbuhl (2013), The long precursory phase of most large interplate earthquakes, *Nat. Geosci.*, *6*(4), 299–302.

Bourouis, S., and P. Bernard (2007), Evidence for coupled seismic and aseismic fault slip during water injection in the geothermal site of Soultz (France), and implications for seismogenic transients, *Geophys. J. Int.*, *169*(2), 723–732.

Bourouis, S., and F. Cornet (2009), Microseismic activity and fluid fault interactions: Some results from the cCorinth Rift Laboratory (CRL), Greece, *Geophys. J. Int.*, *178*(1), 561–580.

Briole, P., A. Rigo, H. Lyon-Caen, J. Ruegg, K. Papazissi, C. Mitsakaki, A. Balodimou, G. Veis, D. Hatzfeld, and A. Deschamps (2000), Active deformation of the Corinth rift, Greece: Results from repeated global positioning system surveys between 1990 and 1995, *J. Geophys. Res.*, *105*(B11), 25,605–25,625, doi:10.1029/2000JB900148.

Bürgmann, R., D. Schmidt, R. Nadeau, M. d'Alessio, E. Fielding, D. Manaker, T. McEvilly, and M. Murray (2000), Earthquake potential along the northern Hayward Fault, California, *Science*, *289*(5482), 1178–1182.

Chen, K. H., R. M. Nadeau, and R.-J. Rau (2007), Towards a universal rule on the recurrence interval scaling of repeating earthquakes?, *Geophys. Res. Lett.*, *34*, L16308, doi:10.1029/2007GL030554.

Chen, K. H., R. Bürgmann, and R. M. Nadeau (2010), Triggering effect of *M* 45 earthquakes on the earthquake cycle of repeating events at Parkfield, California, *Bull. Seismol. Soc. Am.*, *100*(2), 522–531, doi:10.1785/0120080369.

Chen, K. H., R. Bürgmann, and R. M. Nadeau (2013), Do earthquakes talk to each other? Triggering and interaction of repeating sequences at Parkfield, *J. Geophys. Res. Solid Earth*, *118*, 165–182, doi:10.1029/2012JB009486.

Chen, T., and N. Lapusta (2009), Scaling of small repeating earthquakes explained by interaction of seismic and aseismic slip in a rate and state fault model, *J. Geophys. Res.*, *114*, B01311, doi:10.1029/2008JB005749.

Dieterich, J. (1994), A constitutive law for rate of earthquake production and its application to earthquake clustering, *J. Geophys. Res.*, *99*, 2601–2618, doi:10.1029/93JB02581.

Dieterich, J. (1995), Earthquake simulations with time-dependent nucleation and long-range interactions, *Nonlinear Processes Geophys.*, *2*(3/4), 109–120.

Dieterich, J. H. (1979), Modeling of rock friction—1. Experimental results and constitutive equations, *J. Geophys. Res.*, *84*, 2161–2168, doi:10.1029/JB084iB05p02161.

Dieterich, J. H. (1992), Earthquake nucleation on faults with rate and state-dependent strength, *Tectonophysics*, *211*, 115–134.

Dublanchet, P., P. Bernard, and P. Favreau (2013a), Interaction and triggering in a 3D rate-and-state asperity model, *J. Geophys. Res. Solid Earth*, *118*, 2225–2245, doi:10.1002/jgrb.50187.

Dublanchet, P., P. Bernard, and P. Favreau (2013b), Creep modulation of Omori law generated by a Coulomb stress perturbation in a 3-D rate-and-state asperity model, *J. Geophys. Res. Solid Earth*, *118*, 4774–4793, doi:10.1002/jgrb.50311.

Eshelby, J. (1957), The determination of the elastic field of an ellipsoidal inclusion, and related problems, *241*, 376–396

Godano, M., A. Deschamps, S. Lambotte, H. Lyon-Caen, P. Bernard, and F. Pacchiani (2014), Focal mechanisms of earthquake multiplets in the western part of the Corinth rift (Greece): Influence of the velocity model and constraints on the geometry of the active faults, *Geophys. J. Int.*, *197*(3), 1660–1680.

Godano, M., P. Bernard, D. Marsan, and P. Dublanchet (2015), Bayesian inversion of seismic spectral ratio for source scaling. Application to a persistent multiplet in the western Corinth rift, *J. Geophys. Res. Solid Earth*, *120*, 7683–7712, doi:10.1002/2015JB012217.

Hanks, T. C., and H. Kanamori (1979), A moment magnitude scale, *J. Geophys. Res.*, *84*, 2348–2350.

Helmstetter, A., and B. Shaw (2009), Afterslip and aftershocks in the rate-and-state friction law, *J. Geophys. Res.*, *114*, B01308, doi:10.1029/2007JB005077.

Hillers, G., Y. Ben-Zion, and P. Mai (2006), Afterslip and aftershocks in the rate-and-state friction law, *J. Geophys. Res.*, *111*, B01403, doi:10.1029/2005JB003859.

Igarashi, T., T. Matsuzawa, and A. Hasegawa (2003), Repeating earthquakes and interplate aseismic slip in the northeastern Japan subduction zone, *J. Geophys. Res.*, *B5*, 2249, doi:10.1029/2002JB001920.

Kato, N. (2009), A possible explanation for difference in stress drop between intraplate and interplate earthquakes, *Geophys. Res. Lett.*, *36*, L23311, doi:10.1029/2009GL040985.

Kato, N (2014), Deterministic chaos in a simulated sequence of slip events on a single isolated asperity, *Geophys. J. Int.*, *198*(2), 727–736, doi:10.1093/gji/ggu157.

Lambotte, S., H. Lyon-Caen, P. Bernard, A. Deschamps, G. Patau, A. Nercessian, F. Pacchiani, S. Bourouis, M. Drilleau, and P. Adamova (2014), Reassessment of the rifting process in the western Corinth rift from relocated seismicity, *Geophys. J. Int.*, *3*, 1822–1844, doi:10.1093/gji/ggu096.

Lengliné, O., and D. Marsan (2009), Inferring the coseismic and postseismic stress changes caused by the 2004 $M_W = 6$ Parkfield earthquake from variations of recurrence times of microearthquakes, *J. Geophys. Res.*, *114*, B10303, doi:10.1029/2008JB006118.

Madariaga, R. (1979), On the relation between seismic moment and stress drop in the presence of stress and strength heterogeneity, *J. Geophys. Res.*, *84*(B5), 2243–2250.

Marone, C. (1998), Laboratory-derived friction laws and their application to seismic faulting, *Annu. Rev. Earth Planet. Sci.*, *26*(1), 643–696.

Matsuzawa, T., T. Igarashi, and A. Hasegawa (2002), Characteristic small-earthquake sequence off Sanriku, northeastern Honshu, Japan, *Geophys. Res. Lett.*, *29*, 1543, doi:10.1029/2001GL014632.

Nadeau, R., and T. McEvilly (1999), Fault slip rates at depth from recurrence intervals of repeating microearthquakes, *Science*, *285*(5428), 718–721.

Nadeau, R., W. Foxall, and T. McEvilly (1995), Clustering and periodic recurrence of microearthquakes on the San Andreas Fault at Parkfield, California, *Science*, *267*(5197), 503–507.

Peng, Z., and Y. Ben-Zion (2005), Spatiotemporal variations of crustal anisotropy from similar events in aftershocks of the 1999 *M*7. 4 Izmit and *M*7. 1 Düzce, Turkey, earthquake sequences, *Geophys. J. Int.*, *160*(3), 1027–1043.

Perfettini, H., and J. Ampuero (2008), Dynamics of a velocity strengthening fault region: Implications for slow earthquakes and postseismic slip, *J. Geophys. Res.*, *113*, B09411, doi:10.1029/2007JB005398.
Rice, J. R. (1993), Spatio-temporal complexity of slip on a fault, *J. Geophys. Res.*, *98*, 9885–9907, doi:10.1029/93JB00191.
Rice, J. R., and Y. Ben-Zion (1996), Slip complexity in earthquake fault models, *Proc. Natl. Acad. Sci. U.S.A.*, *93*(9), 3811–3818.
Rice, J. R., and S. T. Tse (1986), Dynamic motion of a single degree of freedom system following a rate and state dependent friction law, *J. Geophys. Res.*, *91*(B1), 521–530.
Rubin, A., and J. Ampuero (2005), Earthquake nucleation on (aging) rate and state faults, *J. Geophys. Res.*, *110*, B11312, doi:10.1029/2005JB003686.
Ruina, A. L. (1983), Slip instability and state variable friction laws, *J. Geophys. Res.*, *88*, 10,359–10,370.
Schaff, D., G. Beroza, and B. Shaw (1998), Postseismic response of repeating aftershocks, *Geophys. Res. Lett*, *25*(24), 4549–4552.
Ziv, A. (2003), Foreshocks, aftershocks, and remote triggering in quasi-static fault models, *J. Geophys. Res.*, *108*, 2498, doi:10.1029/2002JB002318.
Ziv, A., and A. Cochard (2006), Quasi-dynamic modeling of seismicity on a fault with depth-variable rate-and state-dependent friction, *J. Geophys. Res.*, *111*, B08310, doi:10.1029/2005JB004189.
Ziv, A., and A. Rubin (2003), Implications of rate-and-state friction for properties of aftershock sequence: Quasi-static inherently discrete simulations, *J. Geophys. Res.*, *108*, 2051, doi:10.1029/2001JB001219.